

THE UNIVERSITY OF CALGARY

**Estimation of Operational Forestry Parameters from
SAR Image Texture**

by

Jonathan Wiebe

A THESIS
SUBMITTED TO THE FACULTY OF GRADUATE STUDIES
IN PARTIAL FULFILLMENT OF THE REQUIREMENTS FOR THE
DEGREE OF MASTER OF SCIENCE

DEPARTMENT OF GEOMATICS ENGINEERING

CALGARY, ALBERTA SEPTEMBER, 1998

©Jonathan Wiebe 1998

ABSTRACT

The main objective of this research was to investigate the relationship between synthetic aperture radar image texture and operational forestry parameters. Two other related issues were also investigated: the value of speckle-filtering before measuring the texture and which texture measure (Markov random field texture models or gray level co-occurrence texture statistics) characterized the texture the best. It was found that: there exists a weak relationship between synthetic aperture radar image texture and the operational forestry parameters of rainforest on Vancouver Island, speckle-filtering before collecting texture features was not beneficial and that Markov random field texture models and gray level co-occurrence statistics performed equally well.

Contents

Abstract	iv
List of Tables	vii
List of Figures	viii
Acknowledgement	ix
1 Introduction and Problem Statement	1
1.1 Image Statistics and Scatterer Models	1
1.1.1 Modelling Image Cell Intensity and Speckle	2
1.1.2 The Composite Scatterer Model	3
1.1.3 Multiplicative Noise	3
1.2 Speckle Reduction Techniques	3
1.2.1 Multi-Looking	4
1.2.2 Adaptive Filters	4
1.2.3 Enhanced Adaptive Filters	5
1.2.4 Bayesian Speckle Filtering	5
1.2.5 Adaptive Bayesian Speckle Filtering with Structure Detection	6
1.3 Summary of Forest Imaging with SAR	7
1.3.1 Forest Backscatter Variability and Texture	7
1.4 Texture Modelling	8
1.4.1 Texture Definitions	8
1.4.2 Texture Models for Forested Scenes	9
1.4.3 MRF Texture Models	9
1.4.4 Grey-Level Co-occurrence Matrix	11
1.4.5 Incorporating Speckle In The Texture Model	11
1.5 Research Objectives	11
1.6 Hypothesis Statements	12
2 Data and Study Site	13
3 Methodology	17
3.1 Data Preparation	17
3.2 Speckle Filtering	17
3.3 SAR Image Texture Estimation	20
3.3.1 MRF Probability Modelling	21
3.3.2 MRF Parameter Estimation	22
3.3.3 MRF Model Order	23
3.3.4 GLCM Feature Set and Offset	23
3.4 Experimental Design	23
3.4.1 Hypothesis Testing	24
3.4.2 Multivariate Analysis of Variance	24
3.4.3 The Fisher Criterion	25
3.4.4 Classification Accuracy	25

4	Results and Discussion	26
4.1	Hypothesis 2: Gamma-Gamma MAP Speckle-Filtering	26
4.1.1	Results	26
4.1.2	Discussion	28
4.2	Hypothesis 1: Operational Forestry Parameters' Relationship To Texture	29
4.2.1	Results	29
4.2.2	Discussion	30
4.3	Hypothesis 3: Comparing the Success of MRF and GLCM Texture Features	30
4.3.1	Results	30
4.3.2	Hypothesis 3: Discussion	30
4.4	Non-hypothesized Results	31
4.4.1	Results from a Real Forest	31
4.4.2	Relating Tone and Standard Deviation to Forestry Parameters	33
4.4.3	Uncorrelated MRF and GLCM Texture Features	34
5	Conclusions and Extensions	37
A	SAR Geometry and Resolution	42
A.1	Range Resolution	43
A.2	Azimuth Resolution	43
B	GIS Stand Classes	44

List of Tables

3.1	The MRF order best suited for the unfiltered image is 3 because it has the most minimums.	23
4.1	The correlation coefficients of the MRF texture features and mean and std properties.	34
4.2	The correlation coefficients from the GLCM texture features and mean and std properties.	34
4.3	The correlation coefficients between the MRF and GLCM texture features.	36

List of Figures

1.1	This figure displays an outline of the decisions that the Gamma-Gamma MAP filter must make.	6
1.2	Symmetric neighbours.	10
2.1	Study site with the RADARSAT scene outlined.	13
2.2	The raw RADARSAT image with three GIS coverages outlined.	15
2.3	A portion of the RADARSAT image (coverage F63) with polygons overlaid.	16
3.1	The F64 coverage portion of the RADARSAT image that has been aggressively speckle-filtered and registered.	18
3.2	A canopy profile of old growth Cedar and Hemlock stand.	19
3.3	A canopy profile of old growth Hemlock and Balsam stand.	19
3.4	Gamma-gamma filter with point target detection.	20
3.5	The conservative and aggressive settings for C_F and C_{max} shown on the C_I histogram.	20
3.6	Those cells marked 'p' are cells which may represent a point target, the other cells are surrounding cells.	21
3.7	The histograms of sample image DNs from within 15x15 windows.	21
3.8	Each cell c , in a window L generates a Q_c	22
4.1	MANOVA average test statistics for MRF and GLCM texture features on all three types of images: raw, (con)servatively and (agg)ressively speckle-filtered images. The 99% confidence threshold is also indicated with a straight line.	27
4.2	Average Fisher criteria for MRF and GLCM texture features on all three types of images: raw, (con)servatively and (agg)ressively speckle-filtered images.	27
4.3	The average percentage of correctly classified windows for MRF and GLCM texture features from all three types of images: raw, (con)servatively and (agg)ressively speckle-filtered images.	28
4.4	MANOVA, Fisher and classification results from the raw image	29
4.5	The MANOVA average test statistic for MRF and GLCM texture features from real forest stands.	31
4.6	The average Fisher criterion for MRF and GLCM texture features for real and virtual forest stands.	32
4.7	The average classification accuracy for MRF and GLCM texture features from real and virtual forest stands	32
4.8	MANOVA, Fisher criteria and classification data plotted for mean, standard deviation and texture features. The texture features were taken from the raw image and the mean and standard deviation features were taken from the aggressively speckle-filtered image.	33
4.9	The average classification accuracy comparing the combined mean, std and MRF or GLCM features with the MRF and GLCM texture features from the virtual forest stands.	35
4.10	The average classification accuracy for MRF and GLCM texture features from real forest stands versus a combined classification.	36
A.1	SAR geometry.	42

Acknowledgements

Acknowledgements are given to my supervisors: Dr. Michael Collins and Dr. David Clausi whose advice and leadership. I'd also like to acknowledge my wife, Patricia, for agreeing to move to Calgary and supporting me throughout the good and bad times at school. My thanks are also directed at Scott Martens who took me skiing and scrambling on many weekends which not only introduced me to the mountains, but gave me time to clear my mind of school and fill my mind with more cosmic thoughts.

Chapter 1

Introduction and Problem Statement

How does texture, the spatial arrangement of digital numbers, from a synthetic aperture radar (SAR) image of a forested scene relate to operational forestry parameters determined from an aerial photograph?

Texture measures are image analysis tools which can be used to segment images. Trees (in a forest) have a wide variety of spatial arrangements determined by a number of environmental and human-made conditions. The spatial arrangement of the trees manifests itself as texture in a SAR image and presents an opportunity to apply texture analysis.

SAR remote sensing platforms are particularly beneficial because they can collect information from the forest regardless of time of day or degree of cloud cover. SAR platforms may also offer a variety of imaging conditions through variation in incidence angle, frequency, polarization and resolution which may capture different properties of the scene.

The investigation of SAR texture is valuable to the forestry industry as well as environmental monitoring agencies. These institutions must monitor this natural resource in an expedient and cost effective manner to sustain development. They need to monitor forest depletions, regrowth, cutting, slashing and infrastructure development (e.g. roads, buildings). Preservation requires accurate knowledge of forest stand characteristics and their geographical placement along with information on areas with active forest operations (Murtha, 1996). Operational forestry parameters (which characterize a forest stand) help companies manage their forests. Typical parameters include species, age, height and stocking. Current methods to collect forest information include aerial photograph interpretation. Texture analysis would aid the efforts outlined above and develop remote sensing technology. *This research will investigate the relationship between SAR image texture from forest stands and operational forestry parameters: species composition, age, height and stocking* (as interpreted from an aerial photograph).

The remainder of this chapter reviews the topics of interest to this study and is organized in the following manner. Since the imagery was formed with a SAR system it is important to review SAR image formation, statistics and image models found in §1.1. SAR imagery is subject to a noise-like process called speckle. §1.2 will include a discussion of some speckle reduction techniques. Next, a summary of forest imaging with SAR is presented in §1.3. The goal of this research is to relate forestry parameters to texture, so a portion of the introduction, §1.4, is dedicated to discussing texture models for SAR forested scenes. The next sections in the introduction present research objectives, §1.5, and hypothesis statements, §1.6.

The data and study site are discussed in §2. At this point, a detailed methodology is included (§3). Finally, the results are presented in §4 and conclusions and extensions are found in the last chapter.

1.1 Image Statistics and Scatterer Models

Familiarization with the SAR image statistics and scatter models is important because this knowledge can be incorporated into speckle filters and texture models. The following presents a one dimensional-model of SAR physics which leads to description of two models: the composite scatterer model and multiplicative noise. The physical relationships and mathematics of processing the raw signal received at the antenna into an image is outlined in the appendix, §A on page 42.

1.1.1 Modelling Image Cell Intensity and Speckle

Mathematically (following Ulaby et al. (1982); Collins (1993); Oliver (1991)), we can model the scattered microwave field ξ as the summation of scattering phasors, where each phasor consists of an amplitude and a phase:

$$\xi = \sum_{j=1}^N a_j e^{i\phi_j} \quad (1.1)$$

where a_j is the amplitude from scatterer j , ϕ_j is the phase, N the number of scatterers and $i = \sqrt{-1}$. The vector summation of the real (ξ_r) and complex (ξ_c) components of equation (1.1) is equivalent to a 2D random walk and is the basic process responsible for speckle-noise.

Fully developed Gaussian speckle is formed by a large number of independent scatterers per resolution cell whose phase and amplitude are independent, identically distributed random variables. As well, the scattering volume should be deep enough (compared to the wavelength) that the phase is a random variable with a uniform distribution between $-\pi$ and $+\pi$. With fully developed Gaussian speckle, ξ_r and ξ_c are random variables with normal distributions due to the central limit theorem (large N). Under these conditions the envelope ($|\xi| = (\xi_r^2 + \xi_c^2)^{1/2}$) is therefore Rayleigh distributed

$$p(|\xi|) = \frac{2|\xi|}{\langle |\xi|^2 \rangle} \exp\left(\frac{-|\xi|^2}{\langle |\xi|^2 \rangle}\right) \quad (1.2)$$

The $\langle \cdot \rangle$ symbol denotes ensemble averages (over all realizations of the scatterers). The intensity, $I = |\xi|^2$, is exponentially distributed.

$$p(I) = \langle I \rangle^{-1} \exp\left(\frac{-I}{\langle I \rangle}\right) \quad (1.3)$$

The scattered field received at u (at the sensor) is

$$\xi(u) = \sum_{j=1}^N a_j e^{i\phi_j} h(u - u_j) \quad (1.4)$$

where u_j is the position of the j^{th} scatterer and h is the impulse response. This is an appropriate one dimensional modelling approach because it encompasses the relevant SAR physics (Oliver, 1991).

Using equation (1.4) the intensity becomes

$$I = \sum_{j,k=1}^N a_j a_k^* e^{i(\phi_j - \phi_k)} \times h(u - u_j) h^*(u - u_k) \quad (1.5)$$

where $*$ denotes the complex conjugate. If one takes the ensemble average over all j and k , only the $j = k$ terms will contribute to the sum. The ensemble intensity is then

$$\langle I \rangle = \eta \sum_{j=1}^N \sigma_j |h(u - u_j)|^2 \quad (1.6)$$

where η is a proportionality constant (to compensate for the gain of the antenna) and σ_j is the cross section of scatterer j ($\eta\sigma_j = a_j a_j^*$). Equation (1.6) is similar to the incoherent imaging of the cross section variations. It follows that the intensity of any image cell will vary about the ensemble intensity $\langle I \rangle$ with a negative exponential distribution seen in equation (1.3). The variation of image cell intensity causes a wormy appearance which is known as fully developed Gaussian speckle.

It should be noted that in equation (1.6) there exists a cross section term σ_j . The cross section term is dependent on the scene characteristics. This implies that image intensity behaviour is also dependent on scene characteristics (i.e. when the scene cross section is not uniform). Mathematically we have

$$p(I) = \int_{-\infty}^{\infty} p(\sigma) p(I|\sigma) d\sigma \quad (1.7)$$

where $p(I|\sigma)$ is the conditional probability density function (pdf) of observing intensity I from an image cell with spatially filtered cross section $\sigma = \sigma_j \times |h(u - u_j)|^2$. This pdf is

$$p(I|\sigma) = (\eta\sigma)^{-1} \exp\left(\frac{-I}{\eta\sigma}\right) \quad (1.8)$$

1.1.2 The Composite Scatterer Model

This widely accepted scatterer model suggests that scatterers form patches with physically similar microwave scattering mechanisms (Jao, 1984). A portion of the scene for this model is thought to consist of several physically different patches of scatterers. The radar footprint may cover one patch or pieces of several patches. In addition, the footprint may also cover combinations of entire patches (smaller than the footprint). Thus the image cell statistics are influenced by variation amongst the patches and by the individual image cell's negative exponential distribution. This scattering model provides a basis to develop a statistical model for the cross section variations found amongst the scatterer patches. It has been found that the Gamma distribution fits these cross section fluctuations well (Oliver, 1991). The pdf of the cross section is

$$p(\sigma) = \frac{1}{\sigma} \left(\frac{\nu\sigma}{\langle\sigma\rangle} \right)^\nu \frac{1}{\Gamma(\nu)} \exp\left(\frac{-\nu\sigma}{\langle\sigma\rangle} \right) \quad (1.9)$$

where ν is an order parameter, $\nu = 1/\text{var}(\sigma)$ and $\Gamma(\cdot)$ is the Gamma function. For areas with smooth cross section $\nu \rightarrow \infty$ and for areas with large cross section fluctuations $\nu \rightarrow 0$. Using equations (1.8) and (1.9) in (1.7) we get the K distribution for the image intensity. The pdf of the K distribution is

$$p(I) = \frac{2}{\langle I \rangle} \left(\frac{I}{\langle I \rangle} \right)^{(\nu-1)/2} \frac{1}{\Gamma(\nu)} K_{\nu-1} \left[2 \left(\frac{I}{\langle I \rangle} \right)^{1/2} \right] \quad (1.10)$$

where $K_{\nu-1}$ is the modified Bessel function of order $\nu - 1$. As $\nu \rightarrow \infty$ (the cross section approaches uniformity) the K distribution approaches the negative exponential distribution in equation (1.3) which would be the theoretical distribution for a portion of the scene with constant cross section.

1.1.3 Multiplicative Noise

The multiplicative noise model considers the image cell intensity to be a product of speckle and *reflectivity*, the true cross section of the scene (Ulaby et al., 1986b; Lee, 1981). Multiplicative noise is represented as

$$I = R \times F \quad (1.11)$$

where I is the intensity, R is the reflectivity and F represents the multiplicative speckle noise. This model relies on the assumption that the backscatter amplitude varies slowly relative to the impulse response (Lee, 1981; Sheen and Johnston, 1992; Blacknell and Oliver, 1993). This means that the scatterer cross section changes very little when compared to the width of the impulse response and corresponds to scatterer patches larger than the radar footprint. In equation (1.5) the above statement allows us to take $a_j a_k^*$ outside the summation. We have then

$$I = aa^* \sum_{j,k=1}^N e^{i(\phi_j - \phi_k)} \times h(u - u_j) h^*(u - u_k) \quad (1.12)$$

leaving multiplicative noise where

$$R = aa^* \quad (1.13)$$

and

$$F = \sum_{j,k=1}^N e^{i(\phi_j - \phi_k)} \times h(u - u_j) h^*(u - u_k) \quad (1.14)$$

1.2 Speckle Reduction Techniques

At this point, it is apparent that the intensity of any image cell in a SAR image is formed by recording the backscatter intensity which is, unfortunately, affected by the random process called speckle. Algorithms which extract information from SAR imagery and which need the 'true' backscatter intensity are affected by the distortion caused by speckle. For example, a texture measure's performance, that doesn't account for speckle statistics, may be degraded by speckle. Consequently, many methods to reduce speckle exist.

This section will discuss multi-looking, the original and enhanced versions of the three common adaptive filters, the Bayesian speckle reduction approach and finally speckle reduction based on *maximum a posteriori* (MAP) and

structure detection. The discussion starts with a simple spectral filter, multi-looking, and then proceeds to summarize spatial filters. The spatial filters are introduced starting from the early adaptive filters and progressing to more sophisticated and recent adaptive filters. The final speckle filter summarized is used in this research.

Two definitions should be noted at this point. *Homogeneous* areas are those which have a slowly varying cross section and fully developed speckle. This corresponds to a patch with many independent scatterers. *Heterogeneous* areas are characterized by areas which consist of structure (edges, lines and point targets) and/or texture. A heterogeneous area contains several different patches of scatterers. Heterogeneous areas may have fully developed speckle given a large number of independent scatters. Furthermore, the multiplicative model may not apply in these areas due to the fluctuations in R .

1.2.1 Multi-Looking

This method averages independent realizations of each resolution cell's reflectivity to reduce speckle. However, the drawback to this method is a reduction in spatial resolution. See the Appendix (section A) for more details on the relationships outlined below.

For a SAR image the slant-range and along-track (azimuth) resolutions are achieved by different physical relationships (Porcello et al., 1976). Slant-range resolution (ρ_r) is determined by a relationship between the speed of light (c) and the bandwidth of the signal (W).

$$\rho_r = c/(2W) \quad (1.15)$$

If the bandwidth increases the slant-range resolution decreases. The along-track resolution (ρ_x) is related to the velocity of the platform (v) and the Doppler bandwidth (Δf_D).

$$\rho_x = v/(\Delta f_D) \quad (1.16)$$

This relationship is similar to slant-range resolution - if the Doppler bandwidth increases the along-track resolution decreases.

To generate a number of different realizations of the scene it is feasible to divide the signal and Doppler bandwidths into several intervals. Each interval can generate an image with independent realizations of the speckle. Therefore, to reduce speckle, average realizations of the scene are created through bandwidth division. From the above descriptions of slant-range and along-track resolution the division of the signal and Doppler bandwidths will also cause the resolution to decrease. The final multi-look image is speckle reduced but also suffers from a degradation in resolution.

1.2.2 Adaptive Filters

There exist three widely utilized adaptive speckle filters which attempt to reduce speckle by smoothing homogeneous areas and retaining backscatter fluctuations in less homogeneous areas with less smoothing. These are the *Lee* filter (Lee, 1981), the *Frost* filter (Frost et al., 1982), and *Kuan* filter (Kuan et al., 1987, 1985). The Lee and Kuan filters are based on an image restoration model which gives the minimum mean-square error of the estimated reflectivity compared with the original digital numbers. The Frost filter is derived by minimizing the expected value of the mean square error.

The model for speckle and scene texture is assumed to be multiplicative for the Lee and Kuan filters. They differ because Lee used a Taylor series expansion to linearize the multiplicative noise model. The consequence of this difference only affects the parameter k_{ij} . Note that the coordinates (i, j) denote the center of a window of imagery. The estimated reflectivity, R_{ij} , is a function of the local spatial average, $\langle I_{ij} \rangle$, and the intensity at (i, j) , I_{ij} .

$$R_{ij} = \langle I_{ij} \rangle + k_{ij}(I_{ij} - \langle I_{ij} \rangle), \quad 0 \leq k_{ij} \leq 1 \quad (1.17)$$

For a locally homogeneous area, k_{ij} should be close to 0. Then the *corrected* intensity is equal to the spatially averaged intensity. However, if k_{ij} is large the *corrected* intensity is a function of the weighted average intensity and the weighted original intensity. In this manner the filter tends to preserve texture, edges, lines and point targets with large k_{ij} while spatial averaging homogeneous areas with small k_{ij} .

By minimizing the expected value of the mean square error,

$$\min E[(R - I \otimes h)^2] \quad (1.18)$$

the Frost filter is formed (h is the impulse response of the SAR). This leads to an adaptive impulse response given below

$$h'(i, j) = K\alpha e^{-\alpha|I_{ij}|} \quad (1.19)$$

where K is a normalizing constant and α is a parameter which is related to the homogeneity of the scene. $h'(i, j)$ represents an impulse response that is able to adaptively reduce speckle. The filter is adaptive because α is proportional to the local scene variability, like k_{ij} is for the Lee and Kuan filters.

The commonality between the three filters, pointed out by Lopes et al. (1990b), is that they all use $std(I)/\langle I \rangle$ to adaptively filter the image. std is the standard deviation. The Lee and Kuan filters use k_{ij} which is proportional to $std(I_{ij})/\langle I_{ij} \rangle$. The α parameter, from the Frost filter is also proportional to $std(I_{ij})/\langle I_{ij} \rangle$.

1.2.3 Enhanced Adaptive Filters

The enhanced adaptive filters developed for the Lee, Frost and Kuan filters by Lopes et al. (1990b), are based on the coefficient of variation C_I , defined as $C_I = STD(I)/\langle I \rangle$. The coefficient of variation (CV) has been noted elsewhere to be a strong function of texture (Ulaby et al., 1986a). The enhancement is possible because the Lee, Frost and Kuan filters are also functions of C_I , but were not using this variable to its full potential. There are three situations, defined by Lopes et al. (1990b), which a speckle filter may encounter.

1. **Homogeneous area.** This is a good example of fully developed speckle and multiplicative noise where speckle can easily be separated from the scene. The filter in this case should restore the scene cross section exactly like a Box filter.
2. **Heterogeneous area.** In this situation it is important to preserve the heterogeneous image features such as texture and structure while smoothing speckle. The speckle filter is only applied to the sub-scenes of the heterogeneous area where all three criteria listed below are valid.
 - (a) Fully developed speckle.
 - (b) Multiplicative speckle model.
 - (c) Speckle and scene variability can be separated successfully.
3. **Heterogeneous area without valid model assumptions.** The speckle filter should not attempt to reconstruct these areas because at least one of the filter criteria (listed (a), (b) and (c) above) has not been met.

For the following, define C_F as the coefficient of variation of a perfectly homogeneous area, C_I the coefficient of variation of the area being examined and C_{max} the coefficient of variation which would be calculated given situation 3 listed above. Based on these three definitions, a speckle filter should perform three operations:

1. Spatial averaging if $C_I \leq C_F$.
2. Selective spatial averaging if $C_F > C_I > C_{max}$.
3. Preserve existing features if $C_I > C_{max}$.

C_F has been theoretically determined for homogeneous areas from intensity L-look images to be $1/\sqrt{L}$ (Ulaby et al., 1986a; Lopes et al., 1990b). If determined from homogeneous portions of an image C_F is distributed as a pseudo-Gaussian function (Lopes et al., 1990b).

C_{max} is not easily determined. There is no theoretical threshold for C_{max} . If C_{max} is chosen too large than valuable textural information may be lost because the filter may choose to smooth the area. It may be best to determine C_{max} from a textured area to ensure that area is preserved.

By incorporating these criteria into the Lee, Frost and Kuan filters, their performance was enhanced. The enhanced filters averaged homogeneous areas well and at the same time maintained structure and texture better than the unenhanced versions.

1.2.4 Bayesian Speckle Filtering

Baye's rule states that:

$$p(\sigma|I) = \frac{p(I|\sigma)p(\sigma)}{p(I)} \quad (1.20)$$

where $p(\sigma|I)$ is the pdf of σ , given I , $p(I|\sigma)$ is the pdf of the intensity given the cross section, $p(I)$ is the pdf of the intensity and $p(\sigma)$ is the unknown pdf of the cross section. Bayesian speckle filtering, which attempts to reconstruct

the underlying cross section based on an *a priori* pdf for σ , is described as a *maximum a posteriori*, (MAP) filter. The MAP estimate is determined by finding the maximum of $p(\sigma|I)$. The maximum can be found using calculus as follows in an example.

Firstly, the pdf $p(I)$ is a normalizing constant, see equation (1.7), and can be ignored. Differentiating the right hand side of the natural logarithm of (1.20) with respect to σ yields

$$\frac{\partial}{\partial \sigma} \ln p(I|\sigma) + \frac{\partial}{\partial \sigma} \ln p(\sigma) \quad (1.21)$$

The choice of distribution for $p(\sigma)$ affects the filters behaviour. For example, assuming you have no knowledge of $p(\sigma)$, chose a uniform $p(\sigma)$, which leads to an identity filter (Oliver, 1991). This is because the second term becomes 0 and then (1.21) becomes

$$-\frac{1}{\sigma} + \frac{I}{\eta\sigma^2} \quad (1.22)$$

This is equal to zero (a maximum point) when $\eta\sigma = I$. This is an identity filter, the estimate of the true reflectivity is the intensity. Other choices of $p(\sigma)$ include Kuan et al. (1987) assuming a Gaussian pdf and Lopes et al. (1990a) choosing the Gamma pdf.

1.2.5 Adaptive Bayesian Speckle Filtering with Structure Detection

This approach proposed by (Lopes et al., 1990a) is adaptive and uses a Bayesian approach with the multiplicative speckle model and a gamma distributed radar cross section (see equation (1.9)). The algorithm is illustrated in Figure 1.1. Two thresholds are used in the algorithm: C_{max} and C_F . If the local CV is greater than C_{max} , the window is textured or contains structure. If the local CV is less than C_F , the window is homogeneous.

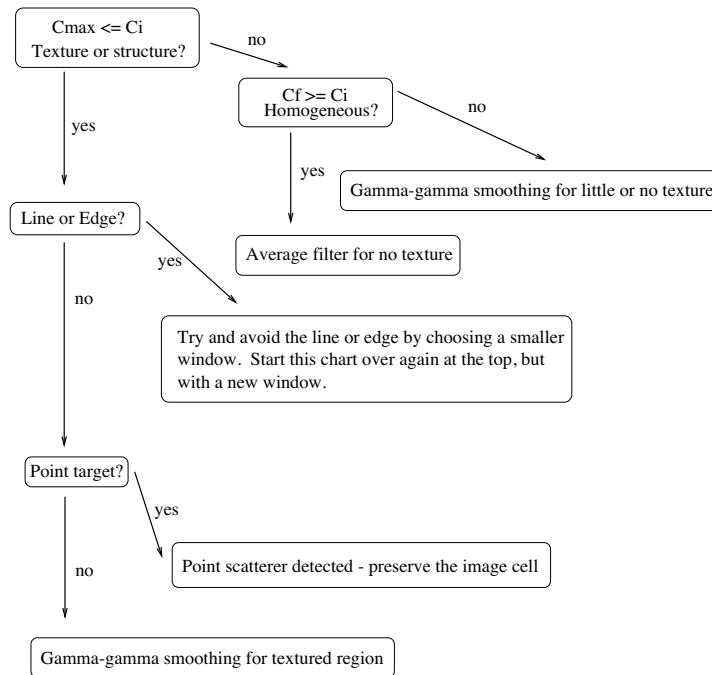


Figure 1.1: This figure displays an outline of the decisions that the Gamma-Gamma MAP filter must make.

Since this algorithm explicitly uses the multiplicative model ($I = R \times F$) it is critical to locate heterogeneous areas where this assumption may not be valid. If the area is heterogeneous it may contain structure or texture. The geometrical ratio detectors are able to detect the heterogeneous areas with structure (edges, lines and points). The local CV is able to detect heterogeneous areas with texture. Initially, a large window is used and assumed homogeneous. It may iteratively become smaller if the window contains edges or lines, until the edge or line is avoided by the window. However, speckle is reduced more effectively with a larger window size, so one should limit how small the window can become. Once the window is considered homogeneous or the window cannot get any

smaller, the reflectivity of the centre image cell is estimated with the adaptive Gamma-Gamma MAP filter. If a point target is detected the image cell intensity is preserved.

Using the Bayesian approach to restore the image, the so called Gamma-Gamma MAP solution (one gamma for $p(\sigma)$ and one gamma for $p(I|\sigma)$) is given by

$$R_{MAP} = \frac{(\alpha - L - 1)\langle R \rangle + \sqrt{\langle R \rangle^2(\alpha - L - 1)^2 + 4\alpha LI\langle R \rangle}}{2\alpha} \quad (1.23)$$

where, $R(= \sigma\eta)$ is the local reflectivity, R_{MAP} is the MAP estimate of the local reflectivity, I is the intensity, L is the number of looks, $\alpha = \frac{1+(C_F)^2}{\langle C_I \rangle^2 - (C_F)^2}$, $C_F = 1/\sqrt{L}$ the coefficient of variation for pure speckle and $C_I = \sigma_I/\langle I \rangle$ the coefficient of variation for a window. In practice $\langle R \rangle$ is estimated by $\langle I \rangle$.

If the scene is homogeneous then $R \rightarrow \langle I \rangle$. Thus $\alpha \rightarrow \infty$ (or $C_I \rightarrow C_F$) and our estimate $R_{MAP} \rightarrow \langle R \rangle$. This makes sense because a good filter for a homogeneous scene is an averaging filter. Conversely when $L \rightarrow \infty$ then $R_{MAP} \rightarrow I$ because a large number of looks effectively reduces the speckle.

1.3 Summary of Forest Imaging with SAR

This research wishes to relate SAR image texture to forestry characteristics. It is useful to present a brief review of forest imaging with SAR. Studies have indicated that SAR is a tool that may be used for forest monitoring and some tree species discrimination. Below is a summary of results from airborne and satellite research on forested scenes.

Airborne SAR studies of forests, in North America, have focused on boreal and eastern forests (Murtha, 1991). This research reveals that multi-date SAR images demonstrate some species age-class discrimination ability and some clear-cut logging mapping uses (Ahern et al., 1993b). Furthermore, combining SAR data with optical data is beneficial for separation of tree species and clear-cut logging mapping (Murtha, 1996). Also, there is some potential for species separation (red/white pine, spruce and jack pine) but logged areas and general forest types are not mapped well by airborne SAR (Murtha, 1996).

Satellite monitoring of forest with RADARSAT SAR have some promising applications. The following information, unless otherwise cited, was found in Ahern et al. (1993a). One promising application is reconnaissance mapping. RADARSAT is able to image at a wide range of incidence angles and is therefore helpful in creating digital elevation models. There is also some potential for coniferous forest species mapping since coniferous forest shows differences in C-band backscatter. Another application of RADARSAT imagery is mapping of logged or burned areas. However, RADARSAT will not be capable of providing timber volume information. C-band (5.3cm) radar scatters mainly from twigs and foliage whereas forest biomass is more closely correlated with tree trunk size. A longer wavelength SAR is needed to correlate the microwave backscatter coefficients to forest biomass and thus timber volume (Le Toan et al., 1992). A final application for RADARSAT is environmental protection. RADARSAT data in combination with other sensors' data and digital elevation models should be able to contribute to a variety of forestry issues: soil conservation, water quality, watershed protection, flood prevention, wildlife habitat and biodiversity.

1.3.1 Forest Backscatter Variability and Texture

What influences microwave (C-band) backscatter from forested scenes? It is known that SAR parameters and scene characteristics influence microwave backscatter intensity. The relationship between neighbouring image cells' intensities results in texture. Thus texture is influenced by phenomena that cause variation in image cell intensity. The SAR parameters which affect intensity include frequency (Hess et al., 1990; Le Toan et al., 1992; Ahern et al., 1995), incidence angle (Sheen and Johnston, 1992; Hess et al., 1990; Rauste, 1990; Ahern et al., 1993a; Cimino et al., 1986), polarization (Hess et al., 1990; Le Toan et al., 1992; Ahern et al., 1995; Wu, 1987), resolution (Sheen and Johnston, 1992; Frost et al., 1984; Woodcock et al., 1988a,b; Woodcock and Strahler, 1987) and speckle (Ulaby et al., 1982; Oliver, 1991; Visentin, 1988). The characteristics of a forested scene which can influence radar backscatter are the environmental factors, (Ahern et al., 1993b; Drieman, 1994), tree species (Le Toan et al., 1992), tree and stand age (Le Toan et al., 1992), human influences (Le Toan et al., 1992) and topography (Rauste, 1990). The following paragraphs outline the characteristics of a forested scene how they affect backscatter. The SAR parameters and speckle which affect intensity are well known and thus further explanations are omitted.

Environmental factors drastically change the characteristics of a forest. Forests can have leaf-on or leaf-off seasons, above or below freezing temperatures, snow or water covered ground, wet or dry snow, changing moisture levels and changing understory. Leaf-on and leaf-off conditions change the number of scatters and the penetration depth of

the radar beam into the canopy. Temperature, snow and water interact and consequently modify the scattering properties of the electromagnetic radiation from the ground and tree elements. The moisture increases the dielectric properties causing wet and dry variations. Seasonal changes can also effect the understory vegetation – growth and dormant periods. Each of the above variations can cause texture differences by modifying backscatter intensity.

Inter-species differences will cause backscatter variability. Tree species have unique trunk-branch structures. Generally coniferous tree species have branches extending in a radial direction while deciduous tree branches are not as well defined. Tree species will also enhance seasonal variation because tree species are affected by seasonal changes differently.

Tree and stand properties are a function of age. As a tree becomes older, trunks become thicker, height increases and the spatial density of trunks decreases. Thus, older stands have a different spatial distribution of tree trunks than stands that are relatively young. This is caused by two processes: competition and common influences (Sayn-Wittgenstein, 1970). Trees require space to develop roots and crowns. Therefore they will dominate their immediate area, which is the *competitive* component. If there are small trees in an area then most likely there will be small trees in the surrounding area. If there are spruce trees in the area then most likely there will be spruce trees in the immediate area. These are *common* influences. Note that common influences and competition are intrinsically related to forestry parameters such as species, age, height and stocking. For example, different species need different amounts of space to develop healthy crowns and roots.

Tree plantations have several characteristics which will affect radar backscatter. Any preferential spatial distribution of trees, such as planting in rows, will change the texture from that of a forest which has been allowed to naturally grow. As well, there are thinning and fertilization practices. Thinning will distort the natural trunk spacing to create an optimal growth environment. Fertilization encourages tree growth in areas which would have not produced as well.

Logging practices will change the forest characteristics as well. Clear cutting, burning and tree planting modify the natural phenomenon of dying, rotting, uncontrolled fires and regrowth.

The local topography changes the scattering properties of the scene. Hills can cause higher intensity backscatter on their radar-near side and obscure forest due to shadow on the far side. Flat areas allow the variability of tree heights to form image texture, rather than the underlying topographical affects.

Attempts to relate forest characteristics (species, age, height, biomass, clearcut, burned) to microwave backscatter have primarily used tonal properties (Le Toan et al., 1992; Ahern et al., 1993b; Kasischke et al., 1994), local standard deviation (Ulaby et al., 1986a; Ahern et al., 1993b; Wu, 1987), frequency distributions (Murtha, 1996) or visual inspection (Ahern et al., 1995; Drieman, 1994) to characterize microwave backscatter. This research proposes that texture measures will successfully extract information about forest characteristics. Some evidence supporting this hypothesis is in the literature. Gray level co-occurrence texture features were tested on three classes of Brazilian forest (virgin, regrowth, clearcut) for discrimination purposes with some success (Luckman et al., 1994). Seasonal changes of Brazilian wetland were indicated by changes in texture on ERS-1 images (Kux and Henebry, 1994).

1.4 Texture Modelling

Texture is defined as the spatial variation of digital numbers within an image. For synthetic aperture radar the variations in digital number are caused by variations in cross section and speckle. More specifically, for a forested scene, evidence presented above, suggests that texture is related to the backscatter fluctuations caused by forest characteristics.

1.4.1 Texture Definitions

A texture measure attempts to characterize the texture within an image. Both natural and human-influenced scenes can have tremendous spatial variability. Consequently, the remotely sensed representation of these scenes will inherit some of that spatial variability. Therefore, a texture measure is required to characterize many types of texture caused by the spatial variability of the scene. The nature of the spatial variation depends on the scene. A highly structured scene contains distinct shapes and periodic structure, like a checkerboard, and will cause highly structured texture. At the opposite extreme the scene may be influenced by random processes, causing an unstructured, random texture.

One model of texture holds that texture is formed by basic texture forming elements called texture primitives (Pratt et al., 1978; Haralick, 1979; Shanmugan et al., 1981). Texture primitives represent a unique spatial relationship between the digital numbers of the image cells. Typically, a texture primitive is a connected set of image cells with uniform digital numbers. However, this is not always the case. Texture primitives may be unconnected and have

image cells with several different digital numbers. The shape of the primitive can be regular (square, triangle) or irregular (blob-like). The spatial density, type and location of texture primitives throughout a neighbourhood determines the type of texture.

Texture measures can be broken down into two categories: structural and statistical (Haralick, 1979). Structural methods to measure texture presume ordered texture. This implies that structural texture analysis methods characterize the texture based on well defined patterns of texture primitives. The statistical methods to measure texture presume neither random nor ordered texture. They use local statistical measures on the digital numbers' spatial arrangement to characterize texture. The local statistical properties will vary with texture, thus enabling one to characterize the texture (Tamura et al., 1978).

The characterization of the texture is in the form of texture features. Texture features are arrays whose elements are related to the texture using numerical values. Each element typically is related to a specific aspect of the texture such as directionality, distance, and correlation. The texture features can be used to cluster the data in feature-space.

1.4.2 Texture Models for Forested Scenes

Since forests exhibit a wide variety of texture (influenced by SAR parameters and forest characteristics), discrimination of forest cover types may be possible based on texture measures. As noted above the appropriate texture measure, sensitive to forest structure, is essential to this operation.

Texture found in forested images is closer to random (i.e. texture with stochastic spatial properties) than ordered. This is verified by considering the number of scatterers and the random placement of the scatterers. Since MRF texture models are statistical and account for random textures, they are assumed to be suitable for forested images.

Since gray level co-occurrence matrices (GLCM) are commonly applied to the interpretation of remotely sensed imagery their results provide a excellent basis to judge the performance of other texture models. Therefore included in the texture analysis will be GLCM features.

1.4.3 MRF Texture Models

Markov random field (MRF) texture models will be applied in this research. A random field is a 2-d lattice of points, where each point is assigned a value based upon a probabilistic model. A MRF is a random field with Markovian properties, i.e. a point's value on the lattice is influenced by other neighbouring values. The specific definition of *neighbours* and their how they influence other points give MRFs the freedom to model many types of textures. MRF texture models for SAR images consider every image cell's backscatter intensity a function of other image cell's intensities in its neighbourhood (Besag, 1974; Chellappa and Chatterjee, 1985). This is intuitively appealing for forested scenes because a tree's spatial position is influenced by its surrounding environment.

The roots of MRFs are found in Ising's model of ferromagnetism (Kindermann and Snell, 1980). The following description of MRFs is a simplified version of a chapter found in Kindermann and Snell (1980). First consider a 1-d series of points $\omega_j, j = 1 \dots N$ with each point being +1 or -1.

$$\omega = (\omega_1, \dots, \omega_N) = (+, +, +, -, -, +, -, +, -, \dots) \quad (1.24)$$

Each point represents a small dipole and the value at each point represents how it is aligned, its' *spin*. If they are all aligned a strong magnetic field is produced, if only some are aligned the magnetic field is weaker. The *energy* at each point, i , is defined as

$$U_i(\omega_i) = \frac{J}{2} \sum_{j \forall |j-i|=1}^N \omega_i \omega_j \quad (1.25)$$

J is a constant. To each combination of the 1-d series of points, ω , let us assign an energy $U(\omega)$, or Gibbs measure.

$$U(\omega) = \sum_{i=1}^N U_i(\omega_i) \quad (1.26)$$

The Gibbs measure, measures the strength of the magnetic field given the spins at each point. Now assign probabilities to each realization of the points with

$$P(\omega) = \frac{e^{-BU(\omega)}}{Z} \quad (1.27)$$

5.1	4.2	3.1	4.3	5.2
4.1	2.1	1.1	2.2	4.4
3.2	1.2	c	1.2	3.2
4.4	2.2	1.1	2.1	4.1
5.2	4.3	3.1	4.2	5.1

Figure 1.2: Symmetric neighbours.

where B is a constant and Z a normalizing constant. This could also be written as

$$P(\omega) = \frac{1}{Z} \prod_i^N e^{-BU_i(\omega_i)} \quad (1.28)$$

In words, the probability of a particular configurations of spins is calculated by using the product of all the points energies. This model is Markovian (see Kindermann and Snell (1980) for a proof) in the sense that

$$P(\omega_j = a \mid \text{all other points}) = P(\omega_j = a \mid \text{two closest points}) \quad (1.29)$$

In other words, the probability of a point having value, a given all points on the line is equal to the probability of having the same value but only given the two nearest neighbours.

This model has been extended to texture analysis with several changes.

1. Extend the model from 1-d to 2-d over a lattice of points.
2. Extend from the binary case of 1 and -1 to a set of gray level values.
3. Change the Gibbs measure to something appropriate to digital images.

For for the purposes of texture analysis, let $X(i, j)$ be a random variable which represents the value at (i, j) on an $N \times M$ lattice L . For simplicity we shall index X with only one variable, e.g. $X(n)$ where $n = 1, 2, 3, \dots, N \times M$. For MRFs if point m is a *neighbour* of point n then $P(X(n))$ depends on the value $X(m)$.

A Markov random field is a joint probability density on the set of all possible digital numbers (representing the backscatter) of L such that $p(X(n)) > 0$ and

$$P(X(n) \mid X(m), m = 1, 2, \dots, N \times M, n \neq m) = P(X(n) \mid \text{neighbours of } n) \quad (1.30)$$

For example, assuming that the conditional probability of a specific configuration of DN about point n is Gaussian we have

$$P(X(n) \mid X(m), m \text{ is a neighbour of } n, m \neq n) = \frac{1}{(2\pi\sigma^2)^{-1/2}} \exp(-1/2\sigma(X(n) - \sum \beta_{n,m}(X(m) + X(m')))^2) \quad (1.31)$$

where σ represents the standard deviation and $\beta_{n,m}$ the parameters of the MRF. Note that this equation is similar to equation (1.27) if we disregard the normalizing constant and instead of constant B for each pair of points there are parameters $\beta_{n,m}$. The summation (in the exponential) is taken over all symmetric neighbours of $X(n)$. Symmetric neighbours consist of a pair of image cells the same distance from the center cell, c , but at opposing angles. m' is defined as being symmetric to cell m . Looking at Figure 1.2, the 1.1 entries are symmetric neighbours. The number of parameters (order of the model) depends upon how many symmetric neighbours are used in the model. In Figure 1.2, up to 5th order symmetric neighbours are depicted. For example a 3rd order symmetric MRF model centered on image cell c , would include those cells marked 1.x, 2.x and 3.x and be characterized by six parameters (the 1.1 entries determine one parameter, the 1.2 entries the next parameter, 2.1 entries for the third parameter, etc ...).

The parameters, $\beta_{n,m}$, are used as texture features. Large parameters represent similar image cell values between the neighbours and the centre value. Small parameters represent different values. For instance, a textured image with vertical stripes, will have MRF parameters which are generally large for the neighbourhoods which are in the vertical direction. In the case of Figure 1.2, the parameters generated by the 1.1 neighbourhood would be large.

The parameters need to be estimated from the only realization of the MRF available – the image. Parameter estimation techniques divide the image cells into independent units (each unit considered a realization) and determine parameters from the units. A number of different techniques exist: coding (Cross and Jain, 1983; Besag, 1986, 1974), least squares (Manjunath and Chellappa, 1991; Chellappa and Chatterjee, 1985) and maximum likelihood estimates (Besag, 1986, 1974).

1.4.4 Grey-Level Co-occurrence Matrix

The grey-level co-occurrence matrix (GLCM) is composed of normalized frequencies, P_{ij} . Entry P_{ij} is the probability of gray tones i and j occurring at a relative distance d and angle θ within the image region under consideration (Weszka et al., 1976; Haralick et al., 1973). The matrix is symmetric and θ is usually defined as one of $\{0^\circ, 45^\circ, 90^\circ, 135^\circ\}$. The gray level image is usually quantized to 2^N gray levels where N is the number of bits per pixel. Therefore, the co-occurrence matrix is of dimensions $2^N \times 2^N$. Texture statistics are defined by sums of probabilities from the GLCM such as

$$\begin{aligned}\text{entropy} &= \sum_{i,j} P_{ij} \log P_{ij} \\ \text{dissimilarity} &= \sum_{i,j \text{ and } i \neq j} |i - j| P_{ij} \\ \text{correlation} &= \sum_{i,j} \frac{(i - \mu_x)(j - \mu_y) P_{ij}}{\sigma_x \sigma_y}\end{aligned}$$

Other GLCM statistics have been used: run length, contrast, maximum probability, uniformity, inverse moment and sum of squares. Each statistic represents some characteristic of the texture.

Some properties of texture can be inferred directly from the distribution of the matrix elements (Weszka et al., 1976). For instance, if there exist homogeneous texture primitives (coarse, blob-like texture) which are large compared with the distance one has chosen to use (i.e. primitive dimension is less than d), then digital numbers of the two image cells will tend to be very close. This means the matrix will have a cluster of entries close to the main diagonal. In contrast, if the texture primitives are smaller than d , fine texture, then the matrix entries will be more uniformly spread.

Unlike MRFs, the GLCM does not make assumptions about image statistics. As well, MRFs assume that the image cell gray levels are related and the GLCM does not. These two points allow the MRF texture model to be more closely associated with the physical process of forest growth and the imaging instrument.

1.4.5 Incorporating Speckle In The Texture Model

This research does not follow the processes presented by Oliver (1991) and company in numerous papers (Oliver, 1993; Oliver and Lombardo, 1996; Lombardo and Oliver, 1994) to model SAR image texture. They incorporate speckle into their SAR backscatter models and this eliminates the requirement of speckle reduction techniques. The texture can be measured by estimating model parameters from the data. Thus, a consequence of choosing a single model for this process is that the opportunity to apply a variety of texture measures which prefer a noise-free image is also eliminated.

Instead of a single model, this research develops two models. The first is a speckle model and the second a texture model. A two step process for this research has been chosen: first reduce the speckle and second perform the texture analysis. Texture analysis will also be completed on images without any speckle reduction to help gauge the effects of speckle reduction on the results.

1.5 Research Objectives

Three objectives exist for this thesis. The main objective is to study the relationship between image texture and operational forest parameters. Two other objectives need to be completed before the main objective is met. One objective is to determine a texture measure which models SAR images of forested scenes well. The other is to use a state-of-the-art speckle reduction algorithm on forested images to separate speckle from texture.

To accomplish the main objective this thesis will attempt to demonstrate that correlation exists between operational forestry parameters determined by interpreting an aerial photograph and texture from a SAR image. This will be accomplished by statistically analyzing texture features associated with known forestry parameters.

One task is to apply texture analysis algorithms based on suitable assumptions about the nature of the texture caused by natural growth forest. The spatial structure of natural growth forests (not influenced by humans) lends itself to texture measures capable of characterizing random textures. Research (see §1.4.3, page 9) indicates that MRF texture measures may be well suited for the task.

SAR is a partially coherent imaging system and consequently subject to speckle effects. For SAR, speckle reduction plays an important initial role in image analysis because SAR image cell intensity is a function of two processes: backscatter variability and speckle. Examining the underlying backscatter variation is difficult because the speckle effects tend to obscure it like noise. After performing speckle reduction on the data, the backscatter variation (texture) should dominate the image enabling one to more precisely measure the texture. Another method is to incorporate speckle into the texture measure thus alleviating the need for speckle filters. This approach is not used as discussed in §1.4.5. Thus, an important aspect of this thesis is to utilize a speckle reduction algorithm to filter the image before applying the texture measures.

In the next section, these three objectives are extended to hypotheses.

1.6 Hypothesis Statements

Three hypotheses will be tested. The first hypothesis concerns the relationship of forestry parameters to SAR image texture. The second hypothesis gauges the benefits of applying of speckle reduction before texture analysis. The last hypothesis compares the performance of the MRF texture model to the GLCM statistics.

Hypothesis 1 *Operational forest characteristics such as species, age, height, and stocking, determined through aerial photograph interpretation, are thought to cause a distinctive spatial arrangement of trees which manifests itself as texture in SAR imagery.*

This hypothesis implies that textural features caused by the spatial arrangement of forest cover types are present in SAR images. This statement is supported by evidence which suggests trees influence microwave backscatter, found in §1.3.1. If one tree influences backscatter then a stand of trees will influence backscatter fluctuation or texture.

This hypothesis will be tested on the forest stands in the RADARSAT image using three tools (to be described in the methodology, §3): multivariate analysis of variance, the Fisher criterion and classification. Each tool is able to determine how well each operational forestry parameter is related to texture.

Hypothesis 2 *Speckle reduction will improve the relationship of the texture features to operational forestry parameters.*

The Gamma-Gamma MAP filter will be used in a manner which attempts to preserve texture while reducing the speckle. If successful the uncertainty of the texture features will be reduced which strengthens the relationship of the texture features to the forestry parameters. This can be tested by comparing results from the multivariate analysis of variance, Fisher criterion and classification from raw and speckle-filtered images.

Hypothesis 3 *Markov random field texture features will capture more textural information (related to the operational forestry parameters) than GLCM texture features.*

MRF texture models should be more appropriate for SAR images of forest because the MRF model is easily associated with the natural processes occurring in a forest. This hypothesis can be tested by comparing the results of the multivariate analysis of variance, Fisher criterion and classification. Those texture features best suited to characterize SAR forest texture will have the best results.

Chapter 2

Data and Study Site

The RADARSAT SAR image obtained for this study is a scene from Vancouver Island of forest stands. RADARSAT is a Canadian earth observation satellite equipped with a SAR. RADARSAT limits our study to a single frequency (C-band), single polarization (HH). The scene was imaged on December 6, 1996 with beam type F2 (single look) during a rainstorm. The pixel spacing is 3.125 m and the scene is centered at about 50.6 degrees latitude and -127.4 degrees longitude. The forest stands are located along the east coast of Vancouver Island between Port Hardy and Port McNeill (see figure 2.1). The land is licensed to Western Forest Products Ltd. (WFP).

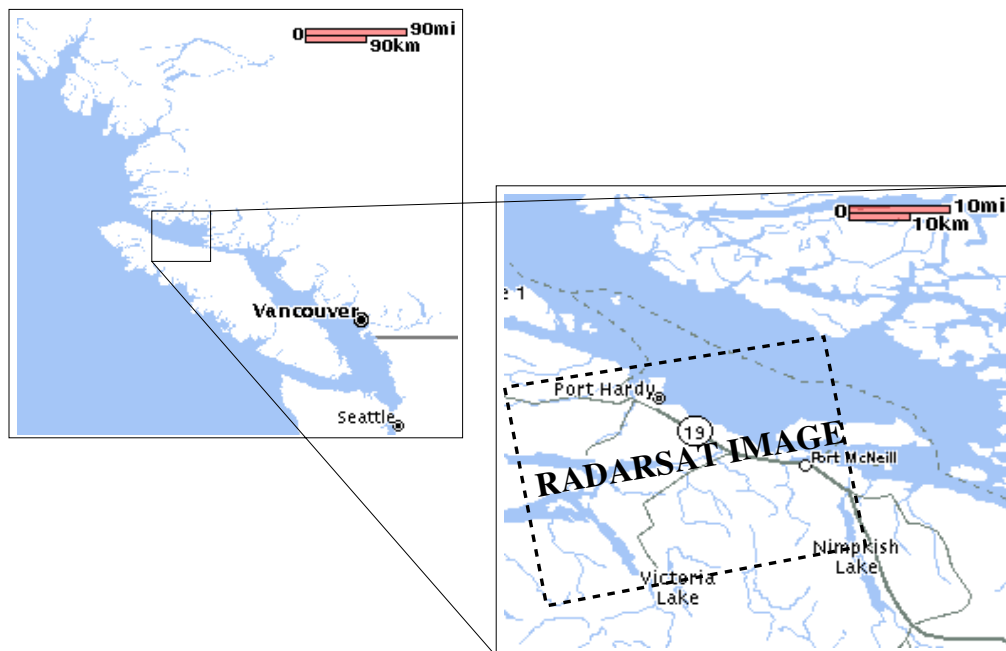


Figure 2.1: Study site with the RADARSAT scene outlined.

To serve as ground truth, a Geographical Information System (GIS) with labelled polygons which detail operational forest parameters was provided by WFP. The GIS labels were formed by aerial photograph interpreters. Each polygon represents the boundary of a forest stand that has at least one unique characteristic which distinguishes it from the neighbouring polygons. Polygon area, perimeter, year established, species composition, age, height, basal area, stocking, UTM coordinates and other information are stored as attribute data for each polygon. This study uses species composition, age, height and stocking data. Figure 2.2 displays the raw RADARSAT image showing three GIS coverages F64, F63 and F54 used in this research. A small sample of polygons (taken from coverage F64) overlaying the image can be seen in Figure 2.3.

The forest stands (outlined by polygons) consist of many different species: Cottonwood, Balsam, Western Red

Cedar, Yellow Cedar, Alder, Douglas Fir, Hemlock, Lodgepole Pine, White Pine and Spruce. The majority of the forest stands are composed of multiple species. The most frequent occurring species are Western red cedar and Western hemlock. The age of the trees ranged from 0 to 250+ years. Each stand was categorized into a stocking (trunk density) class: dense, normal and open. Normal stocking is most common for these stands. Finally, height was also determined and ranged from 1m to 80m. The codes and classes used by the GIS are listed in Appendix B starting on page 44.

The entire RADARSAT image covers two climatic zones: coastal western hemlock and sub-alpine mountain hemlock (Murtha, 1996). The annual precipitation is more than 350cm. The dominant species are Western hemlock, Western red cedar, Sitka spruce and Amabilis fir. The old growth forests have structural characteristics: snags, dead tops, conifers with dome-shaped crowns and spire-shaped crowns of maturing trees (Murtha, 1996).

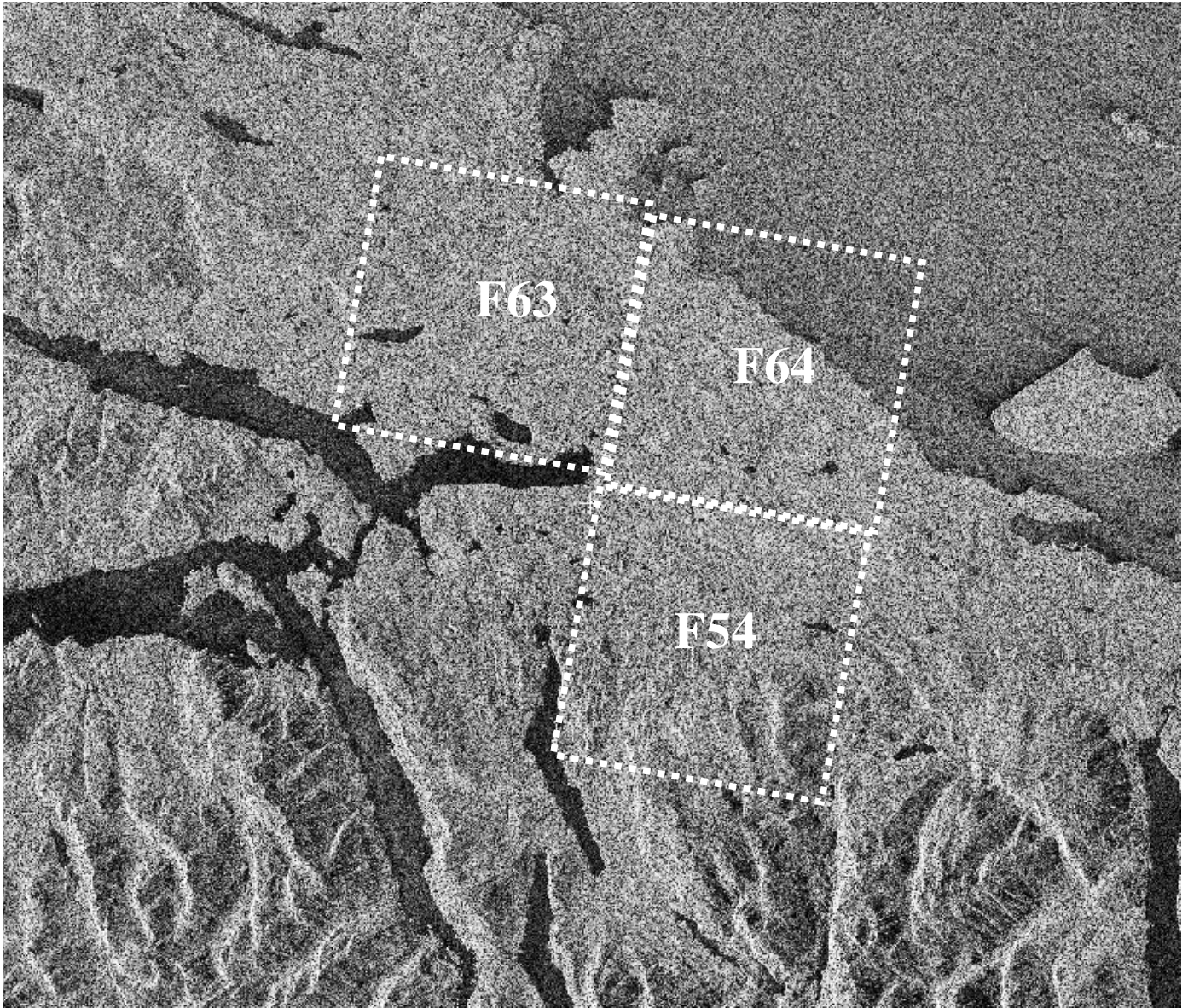


Figure 2.2: The raw RADARSAT image with three GIS coverages outlined.

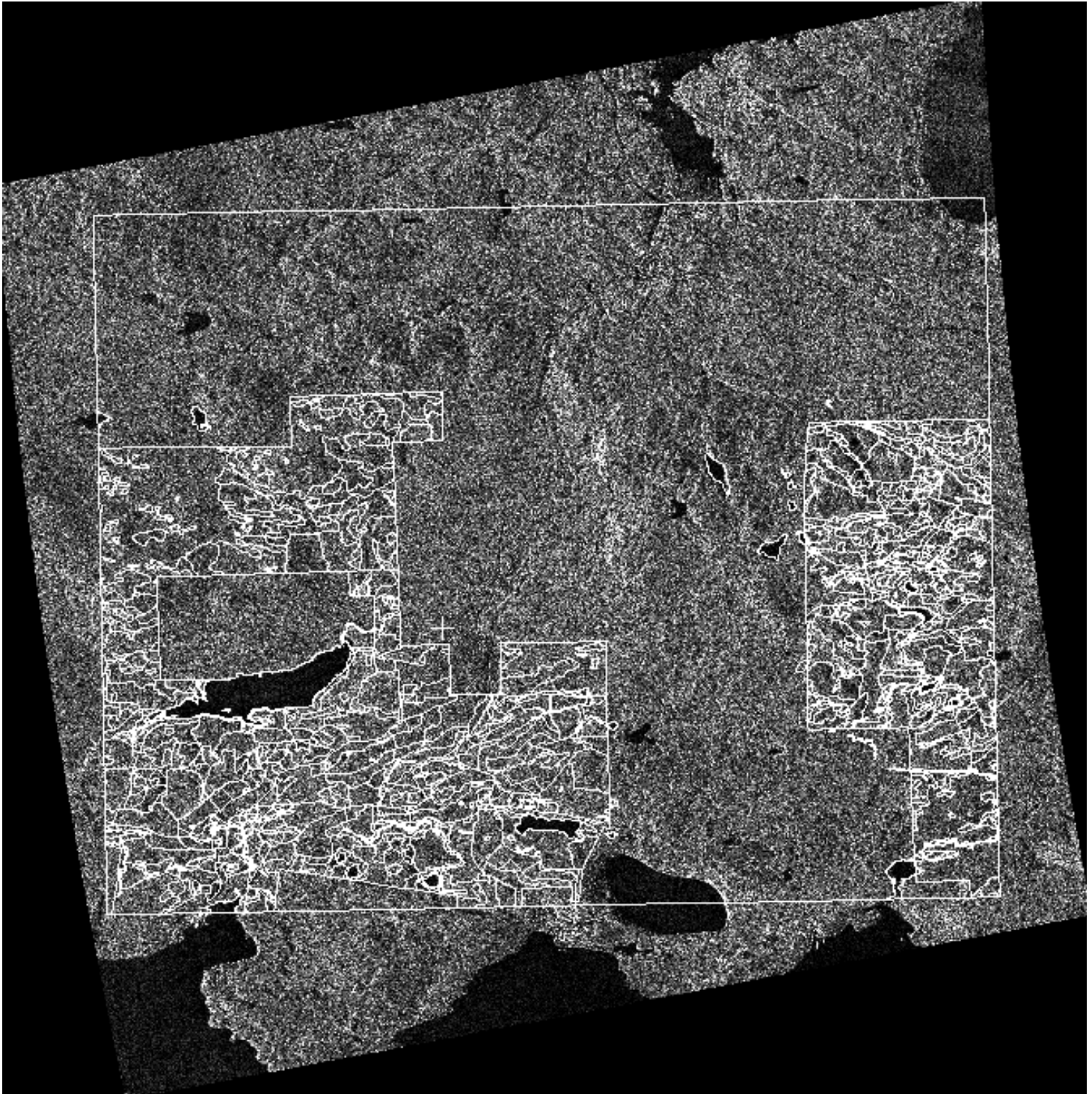


Figure 2.3: A portion of the RADARSAT image (coverage F63) with polygons overlaid.

Chapter 3

Methodology

This section discusses the steps necessary to collect evidence which supports the hypotheses describe in §1.6. The first step prepares the data for analysis and the second presents the details of the implementation of the Gamma-Gamma MAP filter for speckle reduction. The implementation of the MRF and GLCM texture measures are given thirdly. Finally, the experimental design is discussed by presenting the tools used to test the hypotheses.

3.1 Data Preparation

The focus of this section is to describe the data preprocessing necessary to analyze the relationship between texture features and forestry parameters. This required a number of steps which transferred the data between three pieces of software: ARC/INFO, PCI and the texture feature extraction code written by the author. The polygon and associated attribute data was initially received in ARC 'e00' format. The preprocessing steps taken are outlined below.

A coverage is a set of polygons and polygon attribute information. For this dataset the polygons delineate distinct forest types based on forestry parameters such as height, species, stocking and age. Six coverages were received in ARC's 'e00' format and ARC imported them along with their INFO databases. Three attribute fields were added to each coverage which listed species by number instead of letter to enable compatibility between the INFO database and the authors code. The coverages were then exported back to 'e00' format.

The coverages and attribute information were imported by PCI in the 'e00' format to 'pix' vector data. Since the coverages only overlap portions of the full RADARSAT image, the image was subdivided into sub-images which corresponded to the ARC coverages. Unfortunately, of the six coverages available, only three were used because the others did not overlap the image at all or were located over areas with large incidence angle effects (i.e. layover). The RADARSAT sub-images were geocoded using the polygon UTM coordinates and ground control points from lakes and rivers. Figure 3.1 shows a portion of the RADARSAT image that was geocoded.

PCI is able to create mask images with a function called GRDPOL. This function uses the GIS polygons and their attributes to create a mask image. The DNs in a mask image represent properties of the image cells. For instance, an age mask image would consist of image cells with values 1 to 8 which represent 8 different height classes. Three mask files were created for species composition. The first mask file for species delineated the polygons' dominant species. The second and third mask files for species delineated the less dominant species. Mask files were also created for age, height and stocking. These files were important when testing the hypotheses, because it was necessary to combine all forest stands with similar characteristics into a virtual forest (see §3.3 below for the definition of a virtual forest).

3.2 Speckle Filtering

Since SAR images are subject to speckle effects, support for hypothesis 2 was gathered from three versions of an image. The first was the raw image and the second and third images are speckle-filtered in different manners. The Gamma-Gamma MAP speckle filter with structure detection was chosen to filter the second and third images before they were geocoded. Since the only portions of the microwave radar image examined in this research are made of forest stands, it was not necessary to avoid edges or lines which are usually related to human constructs. However, point target detection was retained to preserve the bright backscatter caused by defoliated tree tops (Murtha, 1997). Figure 3.2 shows an example of a forest stand with dead trees, while Figure 3.3 shows a vastly different type of

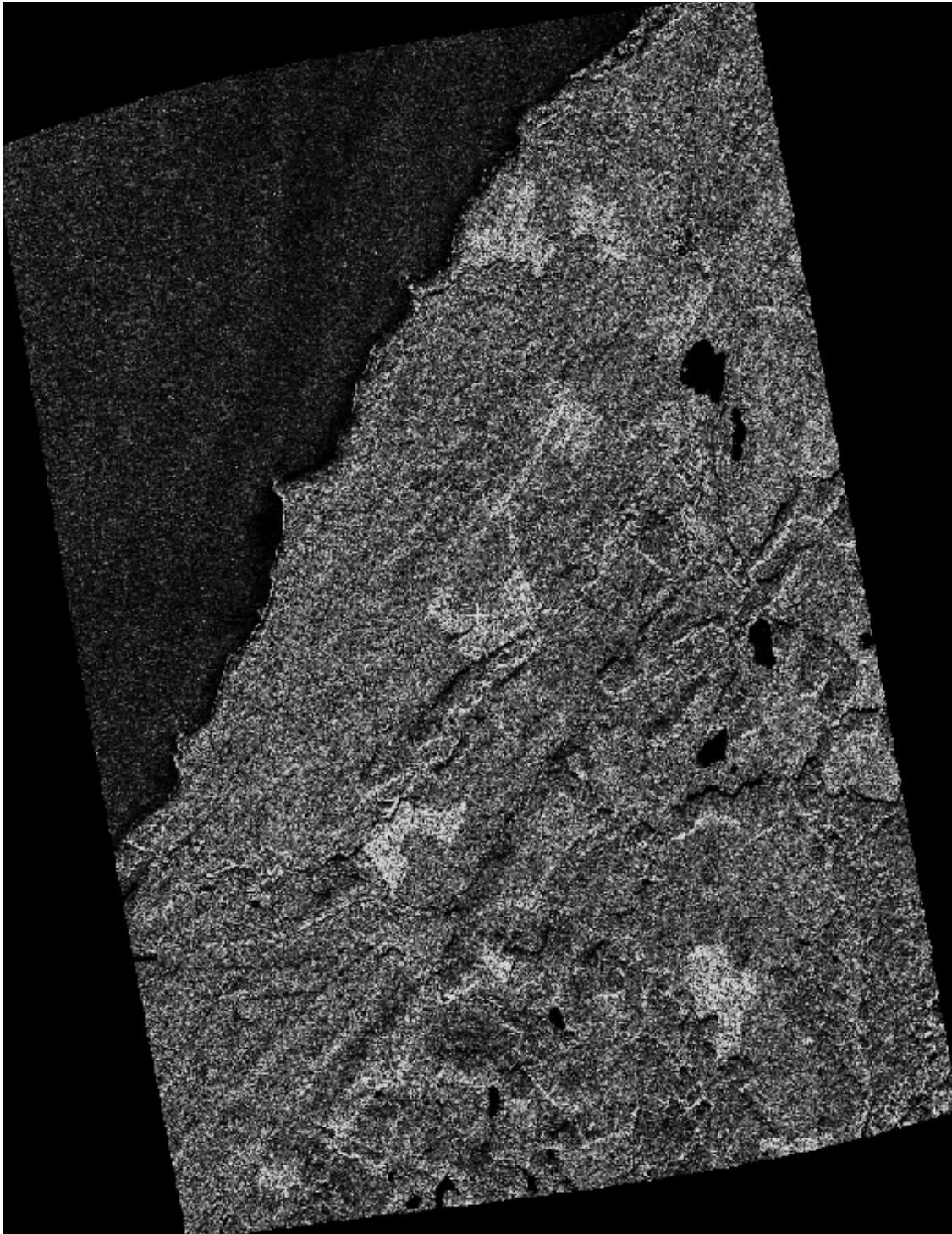


Figure 3.1: The F64 coverage portion of the RADARSAT image that has been aggressively speckle-filtered and registered.



Figure 3.2: A canopy profile of old growth Cedar and Hemlock stand.



Figure 3.3: A canopy profile of old growth Hemlock and Balsam stand.

canopy. Figure 3.4 outlines this implementation of the Gamma-Gamma MAP filter (this figure is similar to Figure 1.1 but without the branches necessary for edge or line detection).

The local coefficient of variation is used in the Gamma-Gamma MAP speckle filter to determine if more or less smoothing of the image is required. The theoretical value of C_F for a one look intensity image is 1. The RADARSAT image is an amplitude image, but by squaring the DN it was transformed to an intensity image for speckle-filtering purposes. However, the mean of our data's C_I is about 0.92, less than C_F . Since it is impossible for our image to be close to pure speckle some of the homogeneous targets were examined (because they should be close to pure speckle). The lakes and ocean gave CV values of about 0.9. Since the weather was stormy on the day the scene was imaged the water must have been rough giving the assumed homogeneous targets (water) heterogeneous features. Therefore, there is no absolute way to determine the level of speckle in the image. A *conservative* speckle filter was used to create the second image by setting $C_F = average(C_I) - 2 * std(C_I)$ and $C_{max} = average(C_I)$. An *aggressive* speckle filter was used to create the third image by setting $C_F = average(C_I)$ and $C_{max} = average(C_I) + 2 * std(C_I)$. See Figure 3.5 for a pictorial placement of C_F and C_{max} on the C_I histogram. Choosing to offset C_F and C_{max} in this manner improved experimental repeatability when using other datasets. The window size of these filters was 7×7 . A larger window is generally better reducing speckle, but because the Gamma-Gamma MAP filter was also expected to preserve texture, a smaller than usual window size was used.

The threshold for point target detection was set to 0.15. This threshold is compared to the inverse ratio of the average of those image cells' DNs which may represent a point target divided by the average of the surrounding image cells' DNs.

$$\frac{\text{average of surrounding image cells}}{\text{average of point target image cells}} \quad (3.1)$$

See Figure 3.6, where "p" represents a cell which may be part of the microwave response to a point scatterer. If the ratio is less than 0.15, then a point target has been detected. The threshold was chosen by firstly generating a binary image of a portion of the scene where 1 meant a point target was detected and 0 meant no point targets were detected. The threshold was varied until most of the point targets, visual to the author, were detected.

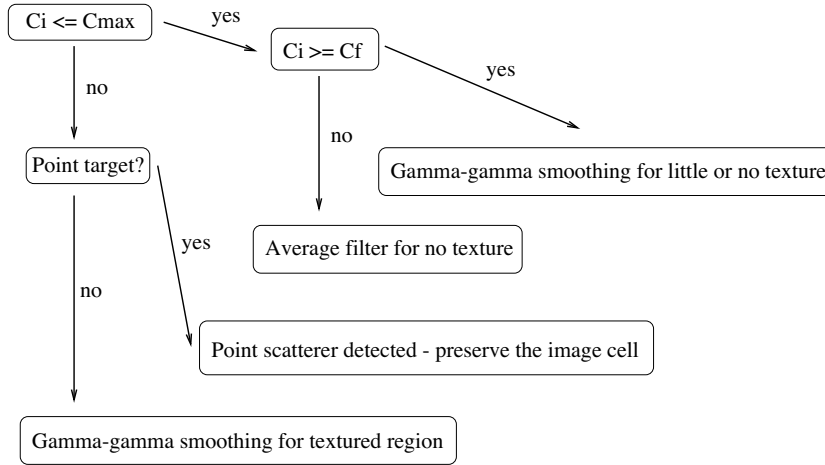


Figure 3.4: Gamma-gamma filter with point target detection.

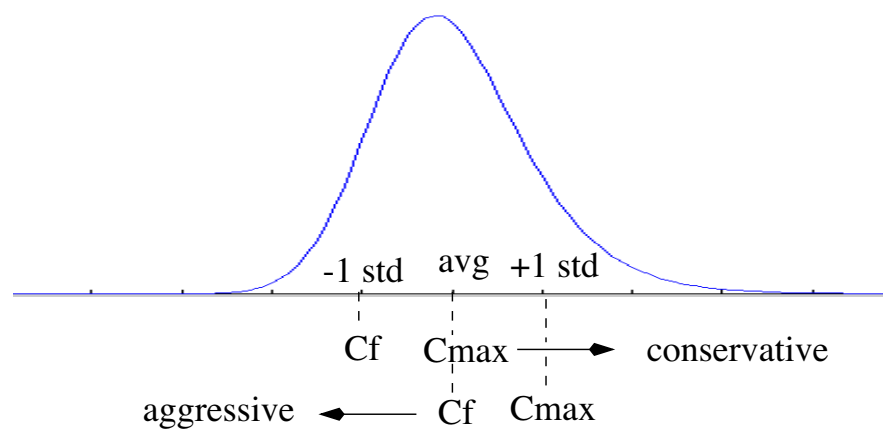


Figure 3.5: The conservative and aggressive settings for C_F and C_{max} shown on the C_I histogram.

3.3 SAR Image Texture Estimation

The texture features (MRF and GLCM) were calculated from within windows, within the polygons. The texture feature collection was done with software coded by the author. This software used a window centered on every fifth image cell to collect the texture features. Using every fifth image cell reduced the computational expense and memory requirements. Furthermore, image cells located on boundaries (more than one type of forest stand in their windows) were ignored. Using the mask files, the texture features from the windows could easily be assigned to virtual forests.

A *virtual forest* is a set of texture features from windows for which all but one forestry parameters are identical. A *virtual forest stand* is a set of windows with identical forestry characteristics. The virtual forest stands make up a virtual forest. For example, suppose all texture features from windows with identical age, species and height were gathered and assigned to a virtual forest. In this particular virtual forest, every stand is identical in age, species and height, but not stocking. Stocking is permitted vary. Now, to test if texture is a function of stocking, one simply has to examine how texture changes as stocking changes within this virtual forest. The virtual forest concept is simply a construct to help organize the forest data into testable subsets. The definition of a real forest is included at this point. A *real forest* is a set of texture features from windows in which all forestry parameters may be different. Using the above example, one would still test how texture changes with stocking, but there is no guarantee that age, height and species will be identical.

MRF texture features characterize the texture better when larger window dimensions, like 32 or 64 (Chellappa and Chatterjee, 1985) are used. Unfortunately window sizes of 32 or 64 would greatly reduce the number of samples

			p			
			p			
		p	p	p		
p	p	p	p	p	p	p
		p	p	p		
			p			
			p			

Figure 3.6: Those cells marked 'p' are cells which may represent a point target, the other cells are surrounding cells.

and, thus, also reduce the number forestry parameter combinations available for study. The larger windows would be more likely to overlap polygon boundaries and, then, subsequently be ignored. A window size of 15x15 was settled upon to comprise between the MRF performance and number of samples.

Three decisions needed to be made concerning the types of MRF and GLCM models. The first is the MRF texture model and second the type of distribution and model order had to be determined. Thirdly, for GLCM, the offset (distance and direction) and feature set needed some consideration.

3.3.1 MRF Probability Modelling

A conditional Gaussian MRF is chosen to model the SAR texture of forest stands. This assumes that the distribution of all image cells within a window (given its' *neighbouring* cells) are Gaussian. The actual image DNs are distributed in an asymmetric manner with the major asymmetry being a longer tail, see Figure 3.7. Other image cell distributions are intractable for MRF modelling and have not been investigated. Other researchers have used the normal assumption when modelling the spatial distribution of trees as mentioned in Besag (1974). One hypothesis of this study predicts that the spatial distribution of the trees will manifest itself as texture, supporting the use of Gaussian MRF. This is the most widely used distribution for MRF models and has been used successfully on many non-normal images. It is assumed that a conditional Gaussian distribution will suffice, but it is a weakness in the theory and the validity of this assumption remains to be tested.

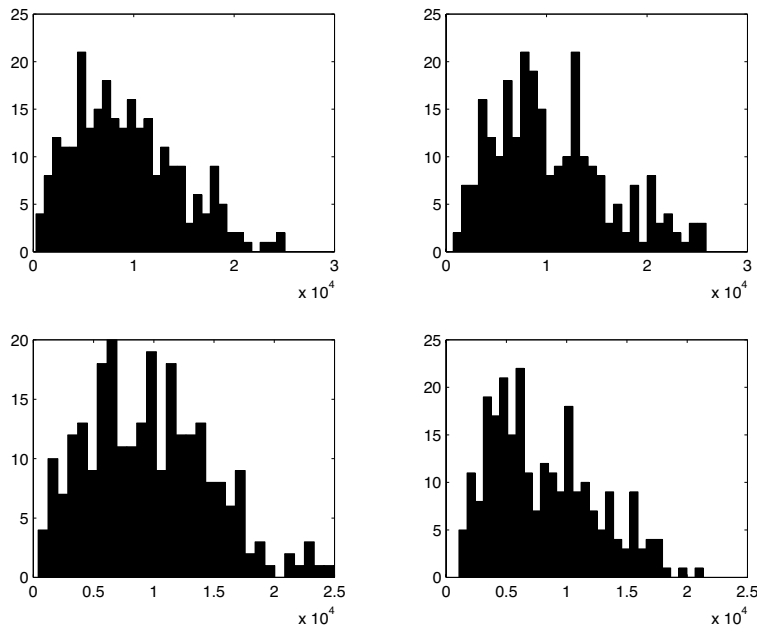


Figure 3.7: The histograms of sample image DNs from within 15x15 windows.

When $p(X(c)|neighbours\ of\ c)$, c being the centre cell of a window, is Gaussian a difference equation can be used

to represent the Markov process (Woods, 1972). The symmetric difference equation is

$$X(c) = \sum_r \beta_{c,r} [X(c+r) + X(c-r)] + e_c \quad (3.2)$$

where e_c is zero mean Gaussian distributed noise, $r = (\delta x, \delta y)$ is an offset from the central image cell c and $\beta_{c,r}$ is a parameter which relates the centre cell to a particular set of symmetric neighbours with offset r . The summation is over all valid values for r , which are determined by the order of the model. For a 2nd order model, the summation would be over two values of r , namely $r = \{(1, 0), (0, 1)\}$. The $X(c-r)$ term is the symmetric neighbour of $X(c+r)$ with $-r = \{(-1, 0), (0, -1)\}$ (see §1.4.3, page 9, for an explanation of order and symmetric neighbours).

3.3.2 MRF Parameter Estimation

The parameters for this study (which become the texture features) are estimated using a least squares approach which is consistent and efficient (Kashyap and Chellappa, 1983; Manjunath and Chellappa, 1991). For the least squares approach, let β be a column vector composed of $\beta_{c,r}$ (one element for each r). Let

$$\mathbf{Q}_c = \begin{bmatrix} X(c+r_1) + X(c-r_1) \\ X(c+r_2) + X(c-r_2) \\ X(c+r_3) + X(c-r_3) \\ \vdots \end{bmatrix} \quad (3.3)$$

where $r_i, i = 1, 2, 3, \dots$ are offsets and the number parameters determines the length \mathbf{Q}_c . If one is working with a 2nd order model, two parameters, then $\{r_1, r_2\} = \{(1, 0), (0, 1)\}$, $\{-r_1, -r_2\} = \{(-1, 0), (0, -1)\}$ and

$$\mathbf{Q}_c = \begin{bmatrix} X(c+r_1) + X(c-r_1) \\ X(c+r_2) + X(c-r_2) \end{bmatrix} \quad (3.4)$$

In matrix notation, Equation (3.2), can be written

$$X(c) = \beta^t \mathbf{Q}_c + e_c \quad (3.5)$$

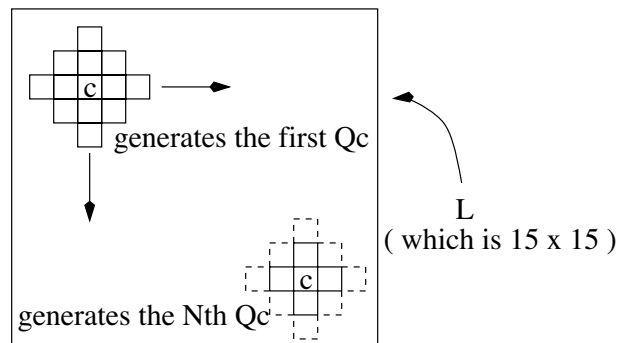


Figure 3.8: Each cell c , in a window L generates a \mathbf{Q}_c

Then, to determine the model parameters $(\beta_{c,r})$, calculate β with the following equation (which is the least squares estimate of β).

$$\beta = \left[\sum_{c \in L} \mathbf{Q}_c \mathbf{Q}_c^t \right]^{-1} \left[\sum_{c \in L} \mathbf{Q}_c X(c) \right] \quad (3.6)$$

The window is represented by L and the summation is over all the cells within L . For this study, L is a 15×15 window and c is any image cell within L . In summation, for every image cell (in the window of texture) a \mathbf{Q}_c is determined. Then for every window the parameter vector β is estimated with Equation (3.6) (see Figure 3.8).

3.3.3 MRF Model Order

When generating texture using MRFs it is apparent that the choice of neighbours and parameter values influence the type of texture created (Chellappa, 1985). For the inverse problem of determining the parameters from the texture the choice of neighbours also plays a crucial role. To help determine the most appropriate order a test statistic is available (Kashyap and Chellappa, 1983; Chellappa, 1985).

The test statistic is able to determine the order which best measures the texture. The test statistic is generated from standard Bayesian theory (Kashyap and Chellappa, 1983) which maximizes $P(\eta_n|\beta)$. Let $\eta_1, \eta_2, \dots, \eta_k$ be the order of different models and m_1, m_2, \dots, m_k be the number of symmetric members. In Figure 1.2, all cells labeled 1.x (where x is 1 or 2), belong to neighbourhood η_1 , all cells labeled 1.x or 2.x belong to neighbourhood η_2 , and, so on, such that all cells labeled $\{i.x|i \leq j\}$ belong to neighbourhood η_j . For example, neighbourhood η_2 contains $m_2 = 4$ symmetric members. Let L be $N \times M$ lattice of points and c is any point on the lattice, $c = (c_1, c_2)$. For any order, say η_n , let $r = (r_1, r_2)$ represent the coordinates of a symmetric member. The test statistic for neighbourhood η_n is then

$$T_n = -2 \sum_{c \in L} \log(1 - \beta_n^t \phi_{nc}) + MN \log(\nu_n) + m_n \log(MN) \quad (3.7)$$

where:

β_n is the column vector of MRF member parameters (or the texture feature vector, as above) for model order n .

ϕ_{nc} is a row vector where each element is determined from $\cos\{2\pi * ((c_1/M, c_2/N) \cdot (r_1/M, r_2/N))\} \forall r \in \eta_n$

ν_n is $\frac{1}{MN} \sum_{c \in L} (X(s) - \beta_n^t \mathbf{Q}_c)^2$

Sym. MRF Order	No Filtering Min.	Con. Filtering Min.	Ag. Filtering Min.
2	0	0	0
3	280	341	299
4	152	85	96
5	9	15	46
Total	441	441	441

Table 3.1: The MRF order best suited for the unfiltered image is 3 because it has the most minimums.

The order with the lowest T_n is the most appropriate for modelling the texture. The data for Table 3.1 is drawn from 441 samples of MRF texture parameters from the unfiltered and filtered RADARSAT images. For each sample, T_n was calculated for 2nd to 5th order symmetric Gaussian MRF. The numbers in the columns represent the number of times an MRF order had the minimum T_n . Table 3.1 shows that 3rd order symmetric MRFs seem to be preferred for unfiltered and filtered RADARSAT fine mode imagery.

3.3.4 GLCM Feature Set and Offset

The GLCM is generated by collected frequencies of gray level pairs at a distance and angle (an offset). The offset as well as the texture statistics generated from the GLCM affect the performance of the texture features (Barber and e. LeDrew, 1991). It has been shown that some features generated from the GLCM are correlated (Ulaby et al., 1986a; Clausi, 1996). In the process of texture analysis using GLCM usually only a few relatively uncorrelated features are best suited for the procedure. Clausi (1996) found that entropy, dissimilarity and correlation were relatively uncorrelated when examining the textural properties of SAR sea ice. This study uses three GLCM features: dissimilarity, entropy and correlation (described in §1.4.4 on page 11). The directions $\{0^\circ, 45^\circ, 90^\circ, 135^\circ\}$ with $d = 1$ were chosen because they are a combination which in the past, have characterized SAR texture well (Barber and e. LeDrew, 1991).

3.4 Experimental Design

The experiments are designed to use three statistical tools which can measure the strength of the relationship between texture features and operational forestry parameters. Each tool measures this relationship in a slightly different manner (as discussed below). Hence, the relationship is examined from three different perspectives.

3.4.1 Hypothesis Testing

Three tools (implemented in MATLAB) were used to examine the relationship between texture and forest parameters: a multivariate analysis of variance (MANOVA), the Fisher criterion and classification. To test, for example, if texture is a function of species, a virtual forest where all forestry parameters are kept constant except species is created. Then for all combinations of species, MANOVA tests, Fisher criteria and classifications are calculated.

MANOVA (Johnson and Wichern, 1992) is able to determine if two datasets have statistically equal or unequal means. For example, if two sets of texture feature data from a virtual forest, identical in every manner but of different height, are proven to have significantly unequal means then this supports hypothesis 1. In other words, this indicates that a change in height has a corresponding change in texture.

The Fisher criterion (Johnson and Wichern, 1992) is the inter-class distance divided by the intra-class variation. This measure represents the separability of the texture features. For example, high separability between virtual forest stands with different stocking indicates that texture is a function of stocking. Moreover, the Fisher criterion places no assumptions upon the distribution of the data, unlike the MANOVA test, as will be mentioned below.

The MANOVA and Fisher criterion are necessary to form conclusions about the relationship between texture and the forestry parameters. In a hypothetical situation where the Fisher criterion failed to indicate strong separability, the MANOVA may still indicate that the texture is significantly different. This would prove that although classification may not be practical, the texture feature vectors are still measuring a change in the texture. In other words, the texture measure is still able to detect any fundamental change in the forest stand properties.

In addition to the MANOVA and the Fisher criterion, a more widely understood measurement, the percentage of windows that were correctly classified with the texture features, was also calculated. Although partially correlated with the Fisher criterion, classification results could support or contradict hypothesis 1, which a wider audience could understand. Furthermore the classification scheme makes Gaussian and equal covariance matrix assumptions which the Fisher criterion does not.

By comparing the test results of from the raw image texture features to the speckle-filtered images, it should be apparent which contained the most textural information. In this manner hypothesis 2 can be tested. Hypothesis 3 is tested in a similar way. The MANOVA test statistics, the Fisher criterion and the success of classification will be lower for the texture measure which characterized the texture the poorest.

A note is included at this point to explain how these tests were used. Note that MANOVA tests statistics could be replaced with the Fisher criterion or the classification accuracy in the following explanation. For a set of virtual forest stands (which compose a virtual forest), MANOVA test statistics for all pairs are calculated and then averaged. For example, take a fictitious set of virtual forest stands { H-2-3-3, H-3-3-3, CB-2-3-3, CB-3-3-3, C-2-3-4 }, where the first letter(s) represent the species (or species composition in the case of two letters), the first number represents age, the second number represents height and the last number represents stocking (species-age-height-stocking). The first virtual forest stand in the set has species code of H, age class 2, height class 3 and stocking class 3. For the species x-label, MANOVA test statistics would be calculated from only two comparisons: H-2-3-3 with CB-2-3-3 and H-3-3-3 with CB-3-3-3. In these comparisons, only the species changes, not the age, height or stocking. The two test statistics would be averaged and plotted above the species x-label. Stand C-2-3-4 could not be used with H-2-3-3 or CB-2-3-3 because its' height is different. For another example, consider the age x-label, where two test statistics would be calculated by using: H-2-3-3 with H-3-3-3 and CB-2-3-3 with CB-3-3-3 in the average. Nothing changes but the age. Unless stated otherwise this labelling is used throughout the results section.

3.4.2 Multivariate Analysis of Variance

This test requires independent samples from two populations. This condition is met by taking samples from independent forest stands (those not adjacent are considered independent). If the sample population size is small, then for a meaningful MANOVA both populations must:

1. be multivariate normal.
2. have equal covariance matrices.

For our forest stands the sample sizes are large (greater than 29, but usually greater than 100) in which case the above assumptions can be relaxed (Johnson and Wichern, 1992). Nevertheless, a random and infrequent comparison of covariance matrices showed only insignificant differences.

Care should be taken when comparing the results of this test between virtual forests. For example, one might have the impulse to suggest that, because the average test statistic for age is higher than the others, age is more closely

correlated with the texture features. This is not the case. The confidence threshold is a constant for all the virtual forests because the number of samples is extremely large and the threshold tends to a constant. The test statistic is not known to be comparable above the threshold; the sample sizes are large, but not equal. It is not acceptable to compare, for example, the test statistics of age and stocking from the same image. However, comparing the same virtual forest stands' test statistics, between images that have been filtered or have been left raw, is acceptable and is done in the results.

3.4.3 The Fisher Criterion

Fisher's idea was to transform the multivariate samples into samples of fewer dimension with linear combinations. A good transformation would achieve the maximum separation between the univariate means. Maximizing a criterion, say $J(w)$, is done to determine the optimal transformation. Let column vectors m_a and m_b represent the means of two classes. Then define

$$S_B = (m_a - m_b)(m_a - m_b)^t \quad (3.8)$$

and

$$S_W = S_a + S_b \quad (3.9)$$

where S_a and S_b are the scatter matrices of the classes a and b . A scatter matrix is defined as

$$S_a = \sum_i (m_a - a_i)(m_a - a_i)^t \quad (3.10)$$

S_B is the squared distance between the class means and S_W is a measure of the variance of the classes. The Fisher criterion is then

$$J(w) = \frac{w^t S_B w}{w^t S_W w} \quad (3.11)$$

where

$$w = S_W^{-1}(m_a - m_b) \quad (3.12)$$

Here, w is the optimal linear combination found by differentiating $J(w)$. For this study, the pairs of sample data used to find a Fisher criterion had uneven numbers of samples which is not taken into account by the Fisher criterion. To improve the situation, the scatter matrices (S_a and S_b) were replaced by covariance matrices (Clausi, 1996).

3.4.4 Classification Accuracy

A weighted Euclidean distance measure was adopted to classify the forest stands. Half the data was used as training data which produced an estimate of the mean and covariance matrix. The other half was classified. For each unique stand of trees, the multivariate mean and variance were calculated. The decision rule for texture features x , given classes A and B follows: given the mean vectors of A and B (m_A and m_B) and the covariance matrices (S_A, S_B), if

$$(x - m_A)S_A^{-1}(x - m_A)^t < (x - m_B)S_B^{-1}(x - m_B)^t \quad (3.13)$$

then x is labelled as class A , otherwise x is labelled as class B . This classification method assumes normality, but because of the large number of samples, this assumption could be relaxed. As well, the best classification was not desired, only a quick estimate was needed to support the MANOVA and Fisher criterion results. This thesis seeks to show how forestry parameters are related to texture and so this classification is only a rough procedure and could potentially be improved.

Chapter 4

Results and Discussion

The overall objective of this research is to establish a relationship between operational forestry parameters and SAR image texture features. This relationship was investigated with three tools: multivariate analysis of variance (MANOVA), Fisher criterion and supervised classification. These tools are able to characterize the relationship between the texture and forestry parameters as strong, weak or nonexistent, and, subsequently, test each hypothesis. This chapter is divided into a number of sections where each presents and discusses the results of each hypothesis test. The test data from the second hypothesis is presented before the first to allow the chapter to flow more naturally from one section to the next. In addition to the results which came directly from the hypotheses, a number of other conclusions also became apparent after some testing. These are given in the last section of this chapter.

4.1 Hypothesis 2: Gamma-Gamma MAP Speckle-Filtering

4.1.1 Results

The average MANOVA test statistics from the MRF texture features are shown on the top graph on Figure 4.1 for all three images: raw, conservatively filtered and aggressively filtered. The x-axis labels represent the type of virtual forest. The y-axis represents the average test statistic. Some of the samples had distributions with elongated tails and standard deviation was not an appropriate value to use for error bars. The error bars indicate the 16% and 84% percentiles. This means that 16% of the samples are below the bottom error bar, 16% of the samples are above the top error bar and 67% of the data is contained within the error bars. The error bars should give a useful impression of the uncertainty.

The 99% confidence threshold is 2.80 for the MRF texture features. The 99% confidence threshold for the GLCM texture features is 2.04. These thresholds are shown as a dashed-dotted horizontal line on the figure. Values greater than these thresholds indicate differences that are significant at the 99% confidence level. The confidence threshold is greater for MRF because the MRF feature vector is 6 dimensional and the GLCM feature vector is 12 dimensional.

The top graph demonstrates that calculating MRF texture features from the raw image is generally better than calculating MRF texture features from the other speckle-filtered images, because the test statistics are higher. This generality is tempered by the large error bars associated with the raw imagery. This trend is true for all the virtual forests except stocking. The average test statistics for stocking are relatively constant for all three types of images.

The GLCM texture features from the raw image are better suited to relate texture to forestry parameters than features derived from the filtered images (see the bottom graph of Figure 4.1, the MANOVA average test statistics for the GLCM texture features). As with the MRF, the error bars are relatively large for GLCM texture features. This diminishes the statistical significance of the differences between the raw and filtered images. Stocking, however, is anomalous because its' test statistics are consistently low for all three types of images. The GLCM results concur with the MRF results.

The Fisher criterion graphs (Figure 4.2) are labeled in the same fashion as the MANOVA graphs, but test statistics are replaced by Fisher criteria. As with the MANOVA figures, the Fisher criteria suggests that the raw image holds more information relating texture to forestry parameters than the conservatively or aggressively speckle-filtered images. This is because texture features (for MRF and GLCM) are more separable when computed from the raw imagery.

As seen on the top graph of Figure 4.3, the MRF texture features from the raw image, in general, were classified

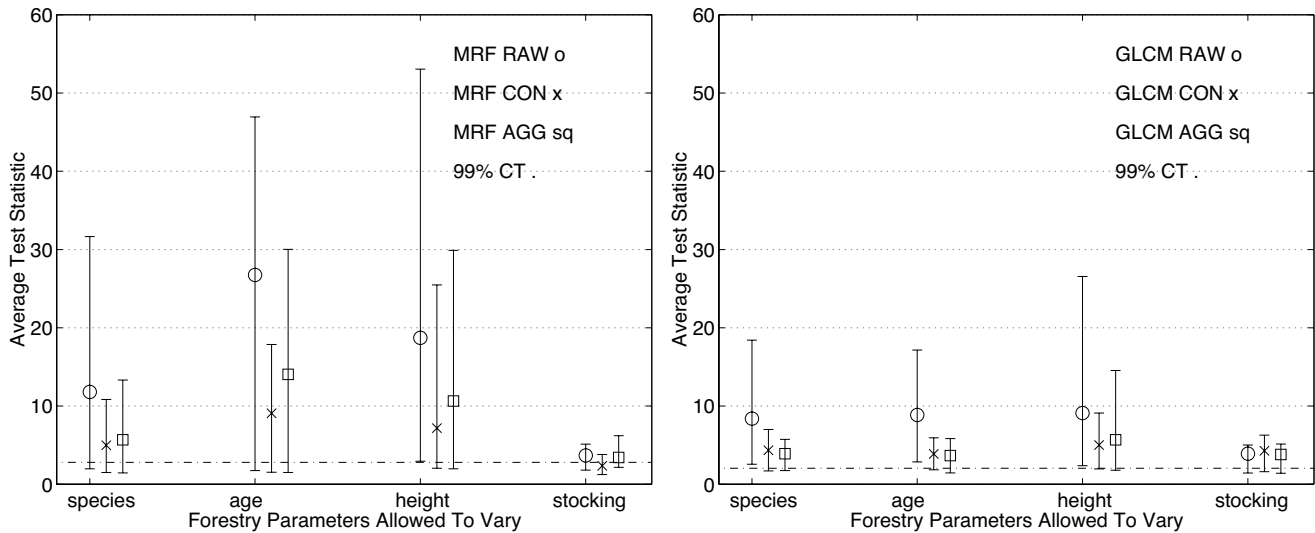


Figure 4.1: MANOVA average test statistics for MRF and GLCM texture features on all three types of images: raw, (con)servatively and (agg)ressively speckle-filtered images. The 99% confidence threshold is also indicated with a straight line.

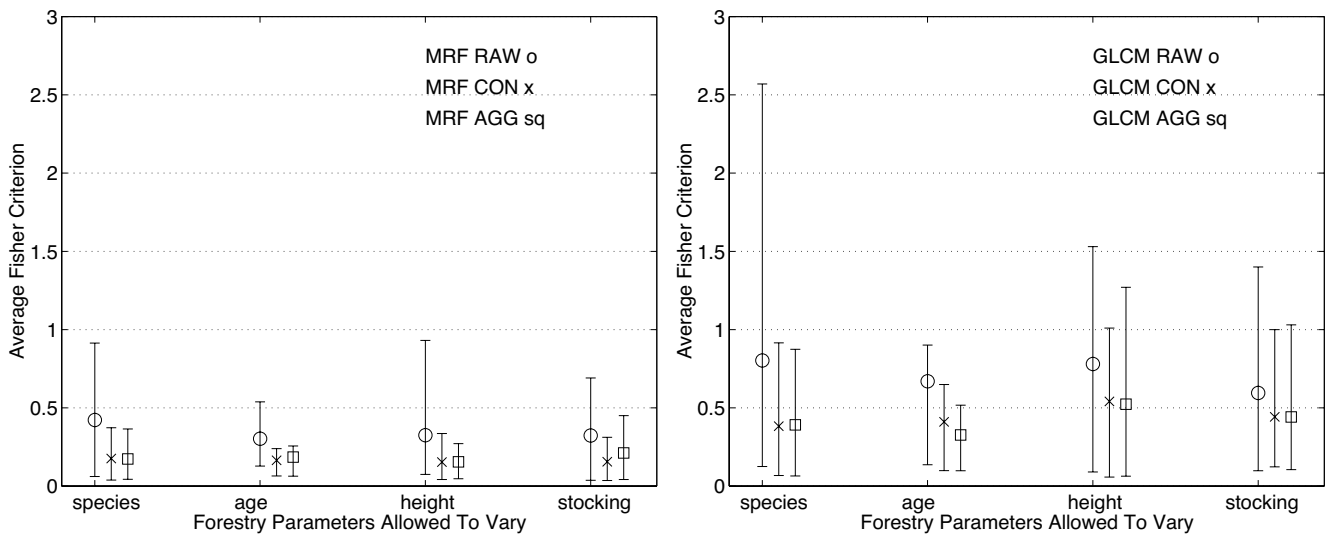


Figure 4.2: Average Fisher criteria for MRF and GLCM texture features on all three types of images: raw, (con)servatively and (agg)ressively speckle-filtered images.

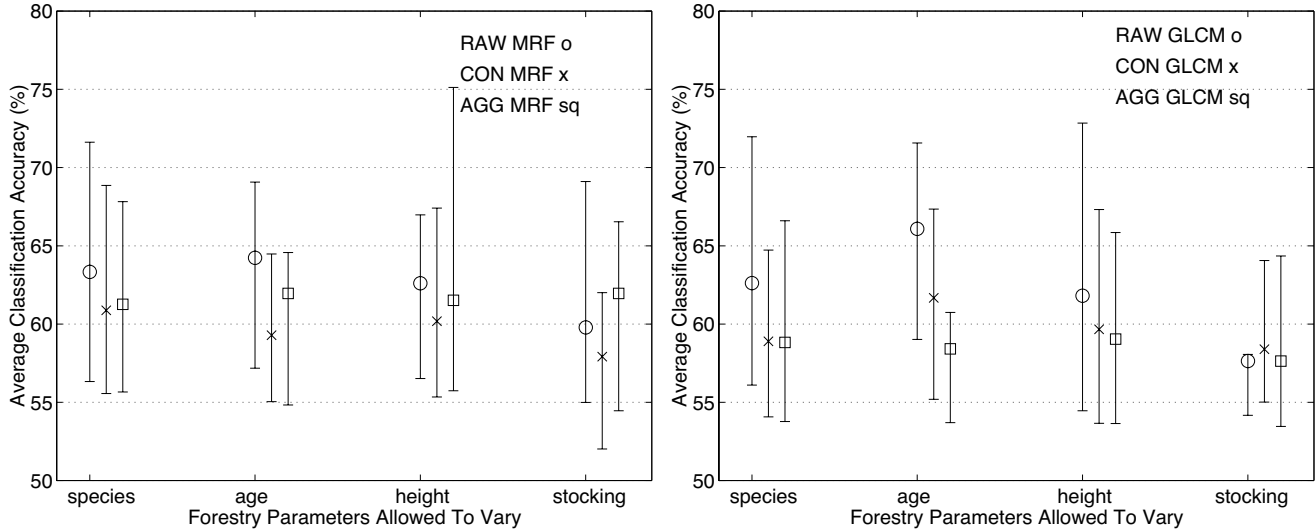


Figure 4.3: The average percentage of correctly classified windows for MRF and GLCM texture features from all three types of images: raw, (con)servatively and (agg)ressively speckle-filtered images.

best. The classification of the aggressively speckle-filtered image MRF texture features show a marked improvement for stocking, which surpassed even the separability of the raw image texture features. Figure 4.3, at the bottom, for GLCM, shows much the same results as the MRF. The raw image texture features have the best overall classification. But, an aggressively speckle-filtered image does not improve the stocking classification as the MRF texture features from the aggressively speckle-filtered imagery did.

4.1.2 Discussion

Data indicates that Gamma-Gamma MAP speckle filtering with point target detect failed to preserve meaningful textural information. The MANOVA, Fisher criterion and classification tests with both texture measures all weakly support this conclusion because the raw image had the most successful results. This failure can be attributed to two possibilities:

1. Inappropriate thresholds chosen for the filter.
2. Erroneous assumptions made by the multiplicative noise model.

Since the image statistics were not close to the theoretical values, *ad hoc* thresholds were chosen for C_F and C_{max} . The Gamma-Gamma MAP filter relies on good choices for C_F and C_{max} and the behaviour of the filter may improve with better threshold values. As well, the point target detection also required a threshold. This was chosen by visual inspection and could be improved.

The multiplicative noise model assumes that the backscatter fluctuations vary slowly relative to the width of the impulse response. This assumption implies that the texture features are a relatively low frequency image property compared to the higher frequency speckle process. Results show that this is not the case with fine resolution RADARSAT imagery. For the imagery in this study, meaningful texture was removed by the filter, along with speckle-noise, implying that texture was not varying slowly enough and the assumption was not appropriate in this case. The limitations of the multiplicative noise model have been outlined by Blacknell and Oliver (1993) in response to a study of forest backscatter by Sheen and Johnston (1992). The failure of the multiplicative noise model suggests that improved speckle reduction and texture preservation methods need to be developed. Otherwise, a unified speckle and texture model, such as discussed in §1.4.5 (on page 11) should be investigated further.

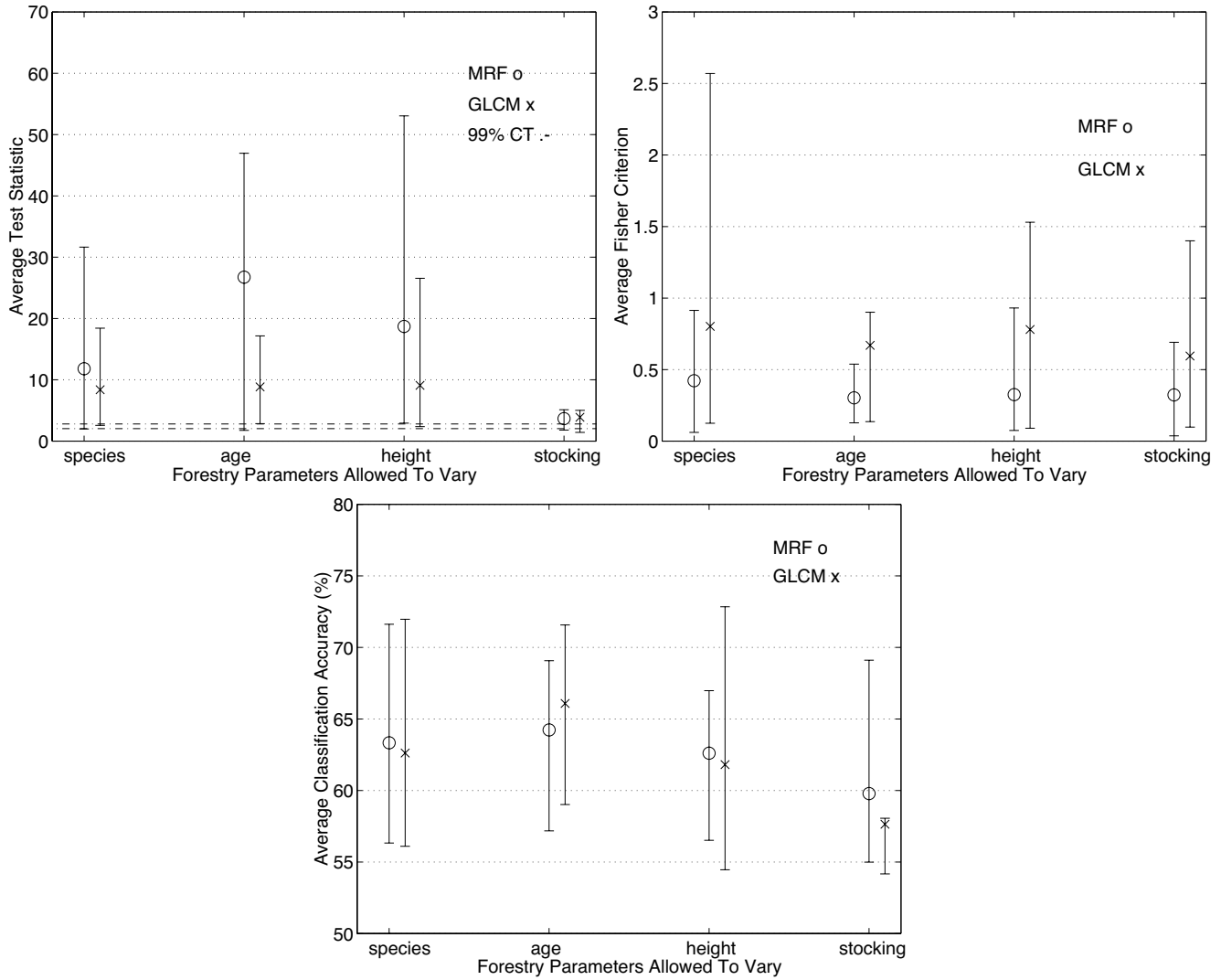


Figure 4.4: MANOVA, Fisher and classification results from the raw image

4.2 Hypothesis 1: Operational Forestry Parameters' Relationship To Texture

4.2.1 Results

As stated in the above discussion, the raw image texture contained the most information relating to operational forestry parameters. Therefore, to demonstrate the results concerning hypothesis 1, only the data from the raw imagery are necessary.

Figure 4.4 plots the average test statistics from the MANOVA tests of the texture features for several virtual forests from the raw image. As noted earlier, the error bars represent the 16% and 84% percentiles. The average of all the virtual forests' test statistics are above these thresholds for MRF and GLCM except for stocking. This indicates that most of the texture feature vectors had large differences in mean. In turn, the large differences in the mean suggest that the texture for each forestry parameter changes as the forest parameter's value changed. This cannot be said for stocking because the average test statistic is too close to the 99% confidence threshold. Note the large error bars, which indicate that not all the the virtual stands were successfully tested.

The second graph from Figure 4.4 plots the average Fisher criterion. For MRF texture features, this figure shows that texture is a slightly stronger function of species than age, height or stocking because the species points are a

little more separable. As well, for MRF the graph indicates that the separability for age, height and stocking is almost constant. For the GLCM texture features the graph is inconclusive because the error bars are too large for all the virtual forests.

The bottom graph on Figure 4.4 details the accuracy of the decision rule used for classification. The overall average classification, using MRF and GLCM texture features, was between 57% and 67% successful. Texture windows with age differences are most accurately classified for MRF and GLCM, but classification of species composition and height are only slightly less accurate.

4.2.2 Discussion

The graphs suggest that the experimental tools have a rudimentary ability to detect changes in texture which reflect changes in species composition, age and height for SAR images of forest stands. The MANOVA and classification tests indicated that stocking is not as well related to texture as the other operational forestry parameters. The Fisher criterion results were inconclusive because none of the forestry parameters were more or less related to the texture features. This relationship is weak as indicated by the large error bars on the MANOVA graphs and the relatively low classification accuracy. Other studies, which attempted to classify forest stands based upon canopy type using texture have achieved comparable accuracies, between 55% and 60%, (for example Ulaby et al. (1986a)). Texture was also successful for age class (virgin and regrowth) discrimination in Brazil (Luckman et al., 1994).

C-band microwaves tend to scatter from the forest canopy (Ahern et al., 1993b, 1995). Therefore changes in the forest canopy structure would cause changes in texture. Changes in canopy structure occur when species composition changes. Thus, it is sensible that SAR texture is related to species. Another consequence of C-band microwaves mainly scattering from the canopy is that shadows are created in the SAR image. Taller trees cast a larger shadow than shorter trees. The texture measures seem to be sensitive to the shadows since texture is related to height. Within a stand of trees, age and height are generally correlated. Trees of the same age will generally be of the same height. Therefore, it is sensible that texture is also related to age. Stocking failed to show even a weak relationship to texture. This is unexpected since the spacing of the tree crowns should relate directly to backscatter fluctuations if the backscatter is mainly from the tree crowns.

The success of this hypothesis demonstrates a new result, being, there is a fundamental relationship between operational forestry parameters (species composition, age and height, but not including stocking) and CHH RADARSAT SAR image texture. This is important because it is a contribution with two corollaries. The first is that SAR image texture, at this scale, is not wholly speckle, but contains spatial information which is related to forestry characteristics. Secondly, it shows that, specifically, this texture is directly related to operational forestry parameters and can be used to help forest stand classification procedures. However, other image properties (tonal, spectral, contextual, etc, ...) should be used in conjunction with texture since texture features are not related to all scene characteristics. This was also concluded by Ulaby et al. (1986a) and Luckman et al. (1994) for, respectively, canopy type and age (virgin or regrowth) classes.

4.3 Hypothesis 3: Comparing the Success of MRF and GLCM Texture Features

4.3.1 Results

Since the MANOVA test statistics are a function of the feature-space dimension, no comparisons are made between MRF and GLCM texture features using test statistics. The Fisher criterion plot, located on Figure 4.4, indicate that the GLCM texture features have slightly more separability than the MRF texture features. The Fisher criteria, again, has large error bars, which weakens our ability to draw conclusions from this result. The MRF errors are smaller than the GLCM error bars. However, the average classification plot, on the same figure, shows that they performed approximately equally well and had comparable error bars (except stocking). MRF texture features were slightly better classified for species composition, height and stocking, but GLCM was better for age.

4.3.2 Hypothesis 3: Discussion

The results for this hypothesis were unexpected. It was hypothesized that MRF texture models would perform better than GLCM, but the graphs indicate that they performed approximately equally well. The Fisher criterion indicated that the GLCM texture features were slightly more separable in feature space, but the classification suggests they

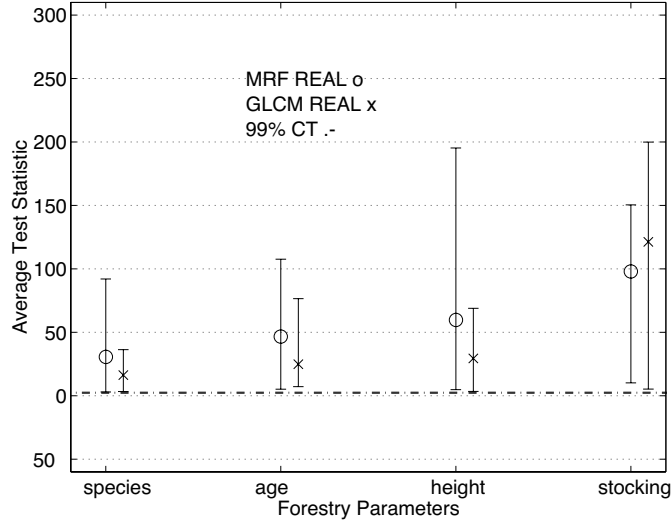


Figure 4.5: The MANOVA average test statistic for MRF and GLCM texture features from real forest stands.

are equally separable. Two explanations exist. The first explanation uses the statistical assumptions made by the Fisher criterion and the classification scheme. The second explanation concerns the conditional distribution chosen for the MRF texture model.

Since the Fisher distance does not assume the data is multivariate normal and the classification scheme does not assume the data is multivariate normal, the different trends that are present in their graphs is not surprising. If the GLCM texture features are non-normal and the MRF texture features are normal, then the Fisher criterion and classification graphs are consistent. The classification scheme penalizes the GLCM texture features because they are not normal, but the Fisher criterion does not penalize the GLCM texture features. Therefore, the GLCM texture features would appear more separable than the MRF texture features when tested with the Fisher criterion, but equal when tested with the classification scheme. This explanation is also consistent with the Fisher criterion and classification data for the aggressively and conservatively speckle-filtered images on Figures 4.2 (on page 27) and 4.3 (on page 28).

The MRF texture model uses a conditional Gaussian distribution to model the texture. As stated in §3.3.1 (on page 21), this is a weakness in the MRF texture model. Since this assumption was not tested, it may have degraded the MRF texture model's performance.

4.4 Non-hypothesized Results

These results were not from any of the hypotheses. While doing the experiments other investigations were carried out. Some of these investigations are considered relevant to this thesis and therefore are discussed below.

4.4.1 Results from a Real Forest

The virtual forest stands established a relationship between the forestry parameters and texture. Do these relationships still exist when the characteristics of the forest stand's being compared are unknown? This is a more realistic situation and involves segmenting forest stands with all forestry parameters able to vary. This type of forest was defined as a real forest. The MANOVA tests on the real forests (Figure 4.5) indicate there exists significant differences in mean for all the forestry parameters. This shows that the relationship between texture and forestry parameters still exists when more uncertainty is added. Figures 4.6 and 4.7 compare the separability (Fisher criterion) and the accuracy of classification of the real forest to the virtual forests. This was only done for the raw image because it had the most promising results. The figures show that the average separability and average classification accuracy for the real forest are lower than the virtual forests. This is not unexpected since texture is a function of many forestry parameters (as shown in §4.2) and a change in texture, for the real forest stands, could be attributed to any number of forestry parameters. The virtual forest constructs eliminated this type of confusion.

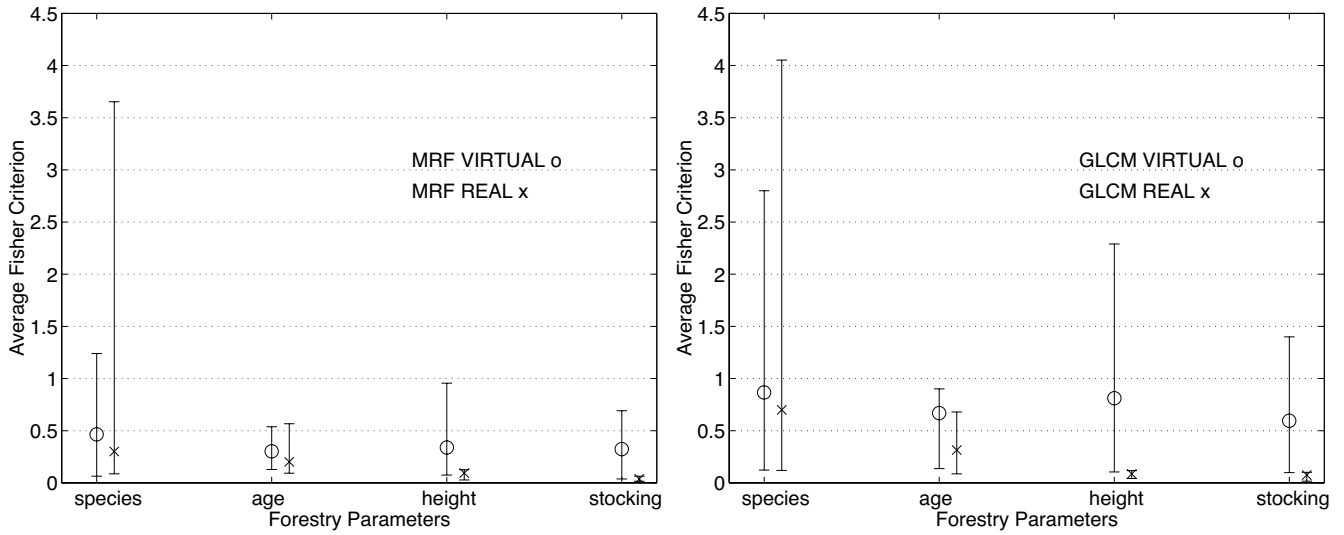


Figure 4.6: The average Fisher criterion for MRF and GLCM texture features for real and virtual forest stands.

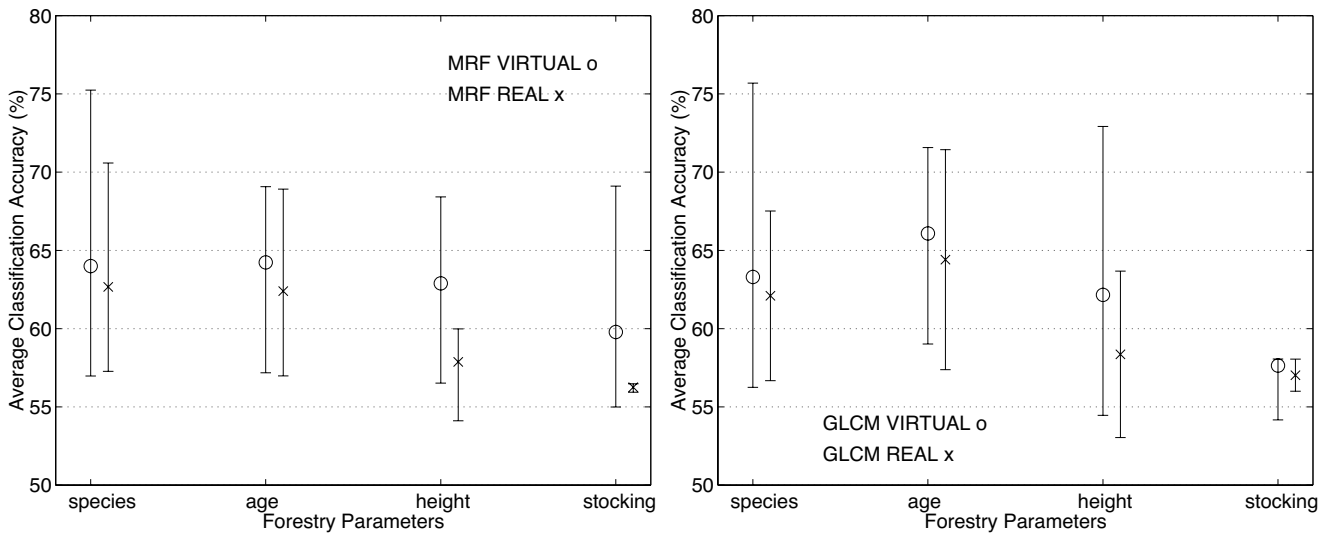


Figure 4.7: The average classification accuracy for MRF and GLCM texture features from real and virtual forest stands

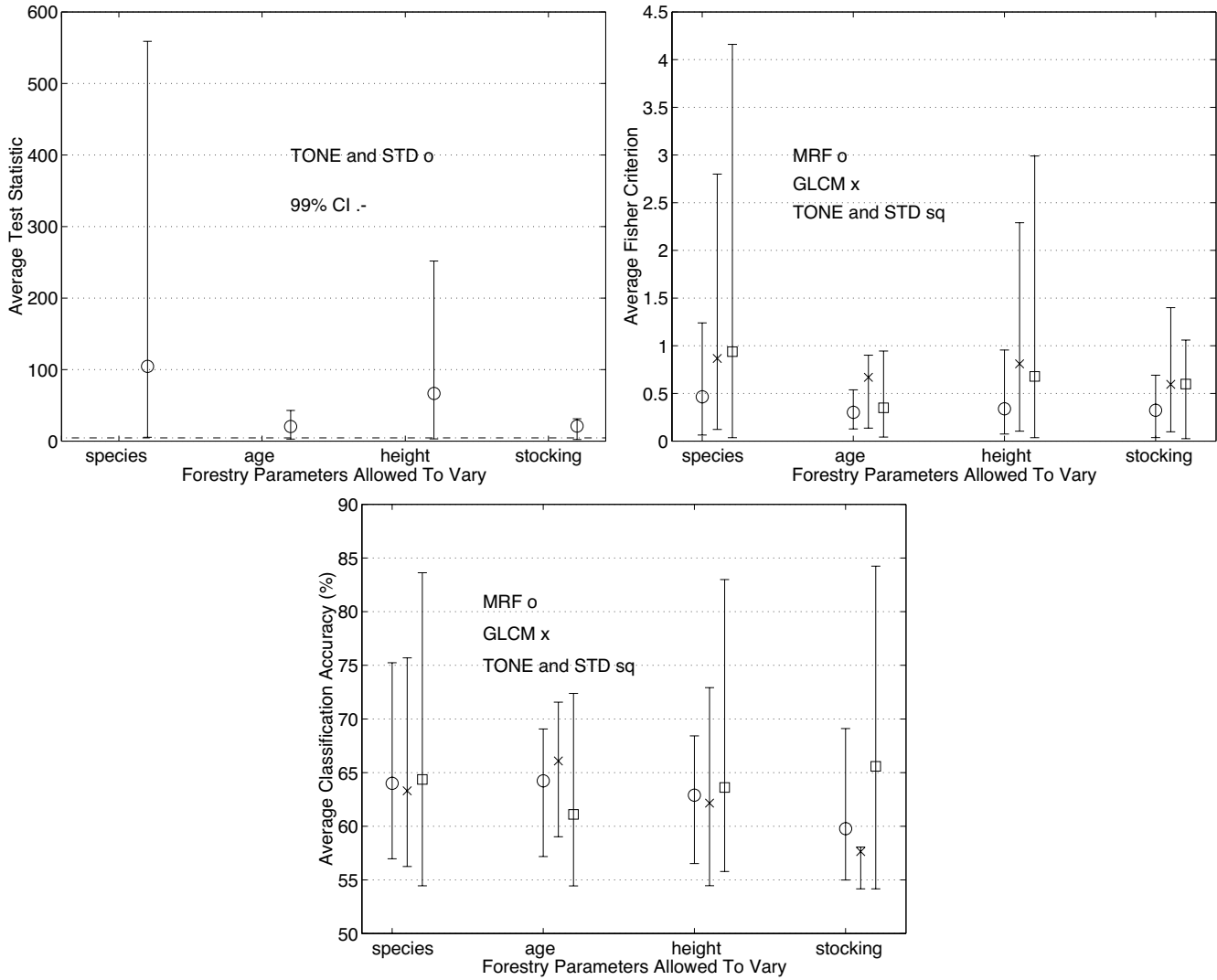


Figure 4.8: MANOVA, Fisher criteria and classification data plotted for mean, standard deviation and texture features. The texture features were taken from the raw image and the mean and standard deviation features were taken from the aggressively speckle-filtered image.

The highest percentage of correctly classified windows for the real forest stands are with age and species for texture features from the MRF texture model and GLCM. This suggests that the greatest potential to successfully segment a real forest into distinct classes with texture features would be into species or age classes. This agrees with the results from testing hypothesis 1, which indicated that texture is a function of species and age.

4.4.2 Relating Tone and Standard Deviation to Forestry Parameters

Is texture providing different information than a simple and faster characterization of the DNs such as mean or standard deviation? The tonal properties of the image can be clearly distinguished, see Figure 3.1 on page 18. For the raw and aggressively speckle-filtered images mean and standard deviation (std) values were calculated from a 15x15 window centred on every 5th image cell, exactly as was done for the texture features. The best Fisher criterion and classification results for the mean and standard deviation were from the aggressively filtered image. This is consistent with previous research which found that spatial smoothing of the image enhanced tonal classification (Ulaby et al., 1986a). Our results (from Figure 4.8) suggest that texture measures and mean and standard deviation are about equally related to forestry parameters. The MANOVA test statistics, at the top on Figure 4.8, show that the mean and std from species and height virtual forest stands are related to forestry parameters. However, age

and stocking points are too close to the confidence threshold to make the same conclusion. Figure 4.8, the middle graph, shows the average Fisher criterion for texture features from the MRF and GLCM measures (from the raw image) and tonal and standard deviation features (from the aggressive image). The tone and standard deviation features had comparable Fisher criteria and classification. Note that stocking stands for mean and std features were most frequently classified correctly. This is not the case for the stocking texture features, which are least frequently classified correctly. Therefore, stocking may be more closely related to mean and standard deviation (std) properties than to textural properties. Finally note that the error bars for the mean and std features are large compared to the texture features, indicating more uncertainty.

Mean and Std	MRF Texture Features					
Features	1	2	3	4	5	6
Mean	0.02	0.00	-0.01	-0.01	-0.04	-0.02
Std	0.01	-0.01	0.01	0.01	0.07	0.08

Table 4.1: The correlation coefficients of the MRF texture features and mean and std properties.

Mean and Std	GLCM Texture Features					
Features	offset x=1 y=0			offset x=1 y=1		
	Entropy	Dissim.	Correl.	Entropy	Dissim.	Correl.
Mean	0.85	0.79	0.32	0.85	0.80	0.31
Std	0.60	0.47	0.57	0.61	0.49	0.57

Mean and Std	GLCM Texture Features					
Features	offset x=0 y=1			offset x=-1 y=1		
	Entropy	Dissim.	Correl.	Entropy	Dissim.	Correl.
Mean	0.85	0.79	0.32	0.84	0.80	0.32
Std	0.60	0.48	0.57	0.61	0.50	0.58

Table 4.2: The correlation coefficients from the GLCM texture features and mean and std properties.

Although being comparable at classification the MRF texture features and the mean and standard deviation properties of the images are uncorrelated, see Table 4.1. The trend is not similar for GLCM texture features, which show high correlation, see Table 4.2. These results suggest that combining the MRF texture features with mean and std features would yield a stronger relationship with the operational forestry parameters. The graphs in Figure 4.9 concur. The combination of MRF, mean and std features are more accurately classified than just MRF features alone. The GLCM classification compared to the combination of mean, std and GLCM features show little improvement. Tonal and std properties are providing different information than the MRF textural properties, as the above evidence suggests. This was also the case in (Luckman et al., 1994), where it was found that tonal features were able to discriminate clearcut areas, while texture features were able to discriminate virgin forest. Ulaby et al. (1986a) found that tonal features performed better than textural features, in contrast to this research, but they used a different set of GLCM statistics and were classifying vastly different canopy types (Brazilian and Eastern US forests) with coarser resolutions (24-looks, 80m \times 80m).

4.4.3 Uncorrelated MRF and GLCM Texture Features

The texture features from the MRF model are uncorrelated with the texture features from the GLCM (see Table 4.3). The MRF texture features are least squares estimates of parameters from a conditional Gaussian distribution. In contrast, the GLCM matrix is the probability of occurrence of two digital numbers and the GLCM statistics are generally summations of the probabilities. The assumptions and measurement of the texture is vastly different for each and thus should not be well correlated.

The low correlation implies that they are characterizing different aspects of the texture and a combined feature set, may give an improved classification. A plot of the classification results between the MRF and GLCM texture features from a real forest versus the combined results show a vast improvement for species. The other types of forest

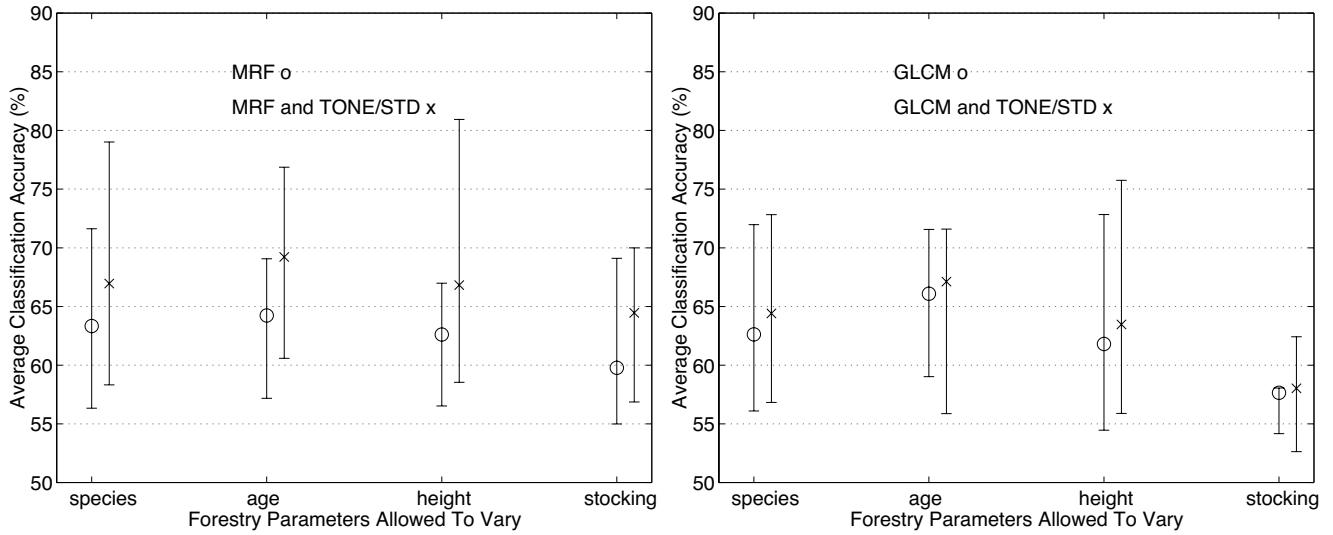


Figure 4.9: The average classification accuracy comparing the combined mean, std and MRF or GLCM features with the MRF and GLCM texture features from the virtual forest stands.

stands show little or even a degradation in classification. This can be seen in Figure 4.10. Why did only species show an improvement, but not the other forestry characteristics? The MRF and GLCM texture features from the species forest stands must be measuring entirely different properties of the image texture, whereas, the texture features from age, height and stocking must be similar.

MRF	GLCM Texture Features					
Texture	offset x=1 y=0			offset x=1 y=1		
Features	Entropy	Dissim.	Correl.	Entropy	Dissim.	Correl.
1	-0.03	-0.11	0.01	0.03	0.04	-0.01
2	0.03	0.09	-0.01	-0.01	-0.02	0.01
3	0.01	0.03	0.01	-0.02	-0.07	0.01
4	0.01	0.02	0.01	0.01	0.02	0.01
5	-0.01	-0.01	0.03	-0.03	-0.05	0.04
6	-0.03	-0.08	0.03	0.01	0.02	0.02

MRF	GLCM Texture Features					
Texture	offset x=0 y=1			offset x=-1 y=1		
Features	Entropy	Dissim.	Correl.	Entropy	Dissim.	Correl.
1	0.05	0.10	-0.01	0.01	-0.00	0.01
2	-0.05	-0.13	-0.01	0.01	0.02	-0.01
3	0.01	0.03	0.01	0.01	0.03	0.01
4	0.01	0.03	0.01	-0.02	-0.07	0.01
5	-0.05	-0.10	0.02	-0.01	0.01	0.02
6	0.01	0.00	0.03	-0.01	-0.03	0.04

Table 4.3: The correlation coefficients between the MRF and GLCM texture features.

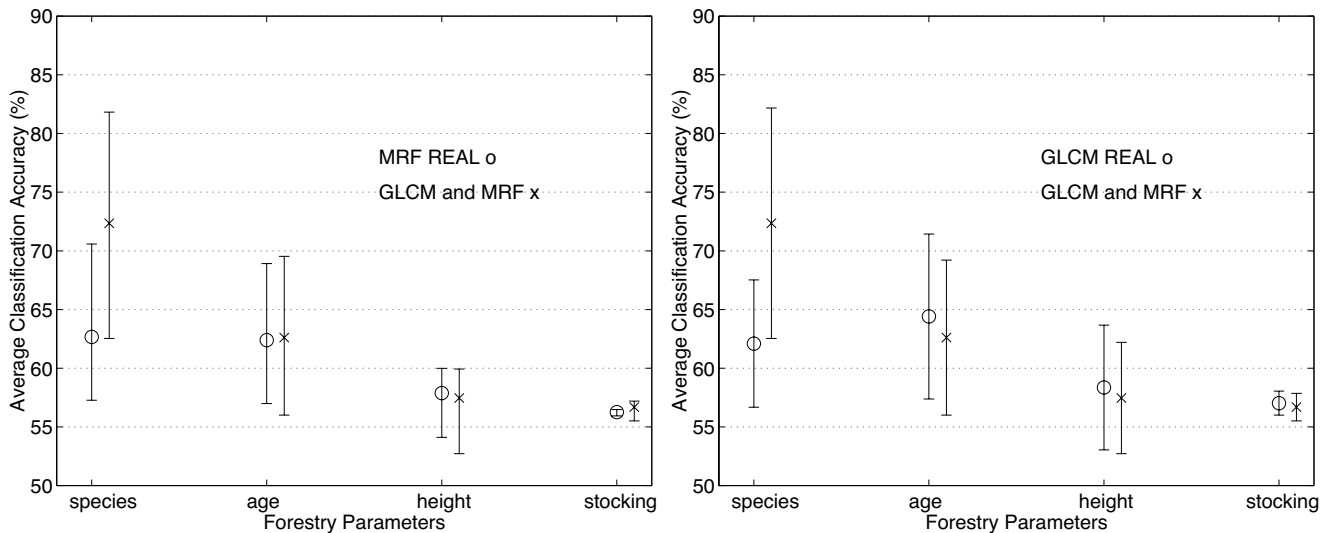


Figure 4.10: The average classification accuracy for MRF and GLCM texture features from real forest stands versus a combined classification.

Chapter 5

Conclusions and Extensions

This research is beneficial to forest monitoring and remote sensing technology. It has related RADARSAT image texture to operational forestry parameters by applying a texture model, Markov random fields. The Markov random field texture features were tested with three statistical tools and compared with another well known texture measure, the grey level co-occurrence matrix statistics. This research also summarized and investigated speckle reduction theory and applied it to forested images.

Several trends are apparent from the figures and comments presented in the results section. These are listed below. The first three follow directly from the hypotheses tests. The last couple were derived from ancillary testing.

1. The texture features, from a RADARSAT F2 image, are related to operational forestry parameters species, age, height. This original result shows that forest scene texture is not wholly speckle, but that it is a function of forestry characteristics. Therefore, texture is useful for forest stand discrimination.
2. The Gamma-Gamma MAP filter with point target detection did not preserve enough meaningful texture. Therefore, the raw imagery showed the best relationship between texture and forestry parameters. This shows that current speckle reduction algorithms may not be preserving valuable textural information and that new or different approaches should be investigated.
3. Neither MRF texture features or GLCM statistics showed any advantages over the other, although it was hypothesized that MRF texture models would perform better than GLCM statistics. It can be concluded that they performed equally well. The failure of hypothesis 3 may be attributed to erroneous normal assumptions made by the statistical tools or a weakness in the Gaussian MRF texture model.
4. The real forest stands did not show as strong a relationship to texture as the virtual forest stands, which was expected. However, age and species composition were classified better than height and stocking, implying that they tend to influence texture more strongly than height and stocking. In general, age and species are stronger influences on texture than height or stocking (in a RADARSAT, F2 image).
5. Mean and std properties are related to forestry parameters and their usefulness for classification is comparable to texture features. Tone should not be overlooked as a valuable image property. This study found that stocking is a stronger function of tonal properties than textural properties.
6. A feature set, composed of MRF texture, mean and standard deviation features classify better than any of these sets on their own. This is because they are all relatively uncorrelated and therefore measuring different image properties. However, GLCM statistics are correlated with mean and standard deviation, and therefore, do not make a valuable feature set.

A number of extensions to this research are listed below.

1. The obvious extension would be to re-classify the features using a more intelligent classification scheme and a feature set consisting of mean, std, MRF textural and GLCM textural properties. The aforementioned image properties have been shown to be uncorrelated and, as such, will improve classification.
2. These conclusions are derived from a RADARSAT image of rainforest on Vancouver Island. The height and species composition of the trees in this climate are vastly different from forests in other climatic zones. At this

point these findings should not be extended to forests in other climates without some caution. If the relative heights and species composition change because of climate the trends demonstrated in this thesis may differ. A logical extension of this research would be to test the same hypotheses on a RADARSAT image of a forested scene from a different climate.

3. Another extension is to acquire RADARSAT images of the same scene at different seasons and during different weather conditions and test the same hypotheses. Seasonal and daily variations in moisture and wind velocity will change the backscatter properties. There may exist a peak season or condition when the textural properties of the scene are more evident. The RADARSAT image used in this study was obtained during a rainstorm. The winds may have distorted the spatial distribution of the tree tops by swaying them. This may have distorted the natural spatial distribution of the tree crowns and thus also affected the textural properties of the image.

Bibliography

- Ahern, F., Leckie, D., and Werle, D. (1993a). Applications of RADARSAT SAR data in forested environments. *Canadian Journal of Remote Sensing*, 19(4):330–337.
- Ahern, F. J., Landry, R., Paterson, J., Boucher, D., and McKirdy, I. (1995). Forest landcover information content of multi-frequency multi-polarized SAR data of a boreal forest. *17th Canadian Symposium on Remote Sensing*, 2:537–549.
- Ahern, F. J., Leckie, D. J., and Drieman, J. A. (1993b). Seasonal changes in relative C-band backscatter of northern forest cover types. *IEEE Transactions on Geoscience and Remote Sensing*, 31(3):668–680.
- Barber, D. and e. LeDrew (1991). SAR sea ice discrimination using texture statistics: A multivariate approach. *Photogrammetric Engineering and Remote Sensing*, 57:385–395.
- Besag, J. (1974). Spatial interaction and the statistical analysis of lattice systems. *Journal of the Royal Statistical Society B*, 36(2):192–236.
- Besag, J. (1986). On the statistical analysis of dirty pictures. *Journal of the Royal Statistical Society B*, 48(3):259–302.
- Blacknell, D. and Oliver, C. J. (1993). Comments on statistical and spatial properties of forest clutter measured with a polarimetric synthetic aperture radar. *IEEE Transactions on Geoscience and Remote Sensing*, 31(5):1093–1094.
- Cenzo, A. D. (1981). Synthetic aperture radar and digital processing: An introduction. Technical Report N81-18266, Jet Propulsion Laboratory, Pasadena, California, USA.
- Chellappa, R. (1985). Two-dimensional discrete Gaussian Markov random field models for image processing. In Kanal, L. N. and Rosenfeld, A., editors, *Machine Intelligence and Pattern Recognition: Progress in Pattern Recognition 2*, volume 1, pages 79–112, B.V. (North-Holland). Elsevier Science Publishers.
- Chellappa, R. and Chatterjee, S. (1985). Classification of textures using Gaussian Markov random fields. *IEEE Transactions on Acoustics, Speech, and Signal Processing*, 33(4):959–963.
- Cimino, J., Brandani, A., Casey, D., Rabassa, J., and Wall, S. D. (1986). Multiple incidence angle SIR-B experiment over Argentina: Mapping of forest units. *IEEE Transactions on Geoscience and Remote Sensing*, 24(4):498–509.
- Clausi, D. (1996). *Texture Segmentation of SAR Sea Ice Imagery*. PhD thesis, University of Waterloo, Systems Design Engineering, Waterloo, Ontario, Canada.
- Collins, M. J. (1993). *Response of an airborne synthetic aperture radar to sea ice in the marginal ice zone*. PhD thesis, York University, Earth and Space Science, Toronto, Ontario, Canada.
- Cross, G. R. and Jain, A. K. (1983). Markov random field texture models. *IEEE Transactions on Pattern Analysis and Machine Intelligence*, 5(1):25–39.
- Drieman, J. A. (1994). Forest cover typing and clearcut mapping in Newfoundland with C-band SAR. *Canadian Journal of Remote Sensing*, 20(1):11–16.
- Fitch, J. P. (1988). *Synthetic Aperture Radar*. Springer-Verlag, New York.
- Frost, V. S., Shanmugan, K. S., and Holtzman, J. C. (1984). The influence of sensor and flight parameters on texture in radar images. *IEEE Transactions on Geoscience and Remote Sensing*, 22(5):440–448.

- Frost, V. S., Stiles, J. A., Shanmugan, K. S., and Holtzman, J. C. (1982). A model for radar images and its application to adaptive digital filtering of multiplicative noise. *IEEE Transactions on Pattern Analysis and Machine Intelligence*, 4(2):157–165.
- Haralick, R. M. (1979). Statistical and structural approaches to texture. *Proceedings IEEE*, 67(5):786–804.
- Haralick, R. M., Shanmugan, K., and Dinstein, I. (1973). Textural features for image classification. *IEEE Transactions on Systems, Man, and Cybernetics*, 3(6):610–621.
- Hess, L., Melack, J., and Simonett, D. (1990). Radar detection of flooding beneath the forest canopy: a review. *International Journal of Remote Sensing*, 11(7):1313–1325.
- Jao, J. K. (1984). Amplitude distribution of composite terrain radar clutter and the k-distribution. *IEEE Transactions on Antennas and Propagation*, 32(10):1049–1061.
- Johnson, R. A. and Wichern, D. W. (1992). *Applied Multivariate Statistical Analysis*. Prentice-Hall Inc., Englewood Cliffs, New Jersey, 3 edition.
- Kashyap, R. and Chellappa, R. (1983). Estimation and choice of neighbors in spatial-interaction models of images. *IEEE Transactions on Information Theory*, 29(1):60–72.
- Kasischke, E., Bourgeau-Chavez, L., N.L. Christensen, J., and Haney, E. (1994). Observations on the sensitivity of ers-1 sar image intensity to changes in aboveground biomass in young loblolly pine forests. *International Journal of Remote Sensing*, 15(1):3–16.
- Kindermann, R. and Snell, J. L. (1980). *Markov Random Fields and their Applications*. American Mathematical Society, United States of America.
- Kuan, D. T., Sawchuk, A. A., Strand, T. C., and Chavel, P. (1985). Adaptive noise filter for images with signal-dependent noise. *IEEE Transactions on Pattern Analysis and Machine Intelligence*, 7(2):165–177.
- Kuan, D. T., Sawchuk, A. A., Strand, T. C., and Chavel, P. (1987). Adaptive restoration of images with speckle. *IEEE Transactions on Acoustics, Speech, and Signal Processing*, 35(3):373–383.
- Kux, H. J. H. and Henebry, G. M. (1994). Multi-scale texture in SAR imagery: landscape dynamics of the Pantanal, Brazil. *IGARSS*, pages 1069–1071.
- Le Toan, T., Beaudoin, A., Roim, J., and Guyon, D. (1992). Relating forest biomass to SAR data. *IEEE Transactions on Geoscience and Remote Sensing*, 30(2):403–411.
- Lee, J.-S. (1981). Speckle analysis and smoothing of synthetic aperture radar images. *Computer Graphics and Image Processing*, 17:24–32.
- Lombardo, P. and Oliver, C. J. (1994). Estimation of texture parameters in k-distributed clutter. *IEE Proceedings - Radar, Sonar and Navigation*, 141(4):196–204.
- Lopes, A., Nezry, E., Touzi, R., and Laur, H. (1990a). Structure detection and statistical adaptive speckle filtering in SAR images. *International Journal of Remote Sensing*, 14(9):1735–1758.
- Lopes, A., Touzi, R., and Nezry, E. (1990b). Adaptive speckle filters and scene heterogeneity. *IEEE Transactions on Geoscience and Remote Sensing*, 28(6):992–1000.
- Luckman, A., Groom, G., and Baker, J. (1994). Forest age discrimination from texture measures of SAR imagery. In *IGARSS 1994*, pages 104–107.
- Manjunath, B. and Chellappa, R. (1991). Unsupervised texture segmentation using Markov random field models. *IEEE Transactions on Pattern Analysis and Machine Intelligence*, 13(5):478–482.
- Murtha, P. (1991). Radar imaging of natural systems (RAINS). ADRO project no. 384.
- Murtha, P. (1996). Airborne SAR studies of north Vancouver Island rainforests. *Canadian Journal of Remote Sensing*, 22(2):175–183.

- Murtha, P. (1997). Radar imaging of natural systems (RAINS). In *GER '97*.
- Oliver, C. J. (1991). Information from SAR images. *Journal of Physics D: Applied Physics*, 24:1493–1514.
- Oliver, C. J. (1993). Optimum texture estimators for SAR clutter. *Journal of Physics D: Applied Physics*, 26:1824–1835.
- Oliver, C. J. and Lombardo, P. (1996). Simultaneous mean and texture edge detection in SAR clutter. *IEE Proceedings - Radar, Sonar and Navigation*, 143(6):391–399.
- Porcello, L. J., Massey, N. G., Innes, R. B., and Marks, J. M. (1976). Speckle reduction in synthetic-aperture radar. *Journal of the Optical Society of America*, 66(11):1305–1311.
- Pratt, W. K., Faugeras, O. D., and Gagalowica, A. (1978). Visual discrimination of stochastic texture fields. *IEEE Transactions on Systems, Man, and Cybernetics*, 8(11):796–804.
- Rauste, Y. (1990). Incidence-angle dependence in forested and non-forested areas in Seasat SAR data. *International Journal of Remote Sensing*, 11(7):1267–1276.
- Sayn-Wittgenstein, L. (1970). Patterns of spatial variation in forests and other natural populations. *Pattern Recognition*, 2:245–253.
- Shanmugan, K. S., Narayanan, V., Frost, V. S., Stiles, J. A., and Holtzman, J. C. (1981). Textural features for radar images analysis. *IEEE Transactions on Geoscience and Remote Sensing*, 19(3):153–156.
- Sheen, D. and Johnston, L. P. (1992). Statistical and spatial properties of forest clutter measured with polarimetric synthetic aperture radar. *IEEE Transactions on Geoscience and Remote Sensing*, 30(3):578–588.
- Tamura, H., Mori, S., and Yamawaki, T. (1978). Textural features corresponding to visual perception. *IEEE Transactions on Systems, Man, and Cybernetics*, 8(6):460–472.
- Ulaby, F. T., Kouyate, F., Brisco, B., and Williams, T. H. L. (1986a). Textural information in SAR images. *IEEE Transactions on Geoscience and Remote Sensing*, 24(2):235–245.
- Ulaby, F. T., Moore, R. K., and Fung, A. K. (1982). *Microwave Remote Sensing Active and Passive Volume II*. Addison-Wesley Publishing Company, Reading, Massachusetts.
- Ulaby, F. T., Moore, R. K., and Fung, A. K. (1986b). *Microwave Remote Sensing Active and Passive Volume III*. Artech House Inc, Canton, MA.
- Visentin, R. L. (1988). A digital signal processing view of strip-mapping synthetic aperture radar. Master's thesis, University of Illinois.
- Weszka, J. S., Dyer, C. R., and Rosenfeld, A. (1976). A comparative study of texture measures for terrain classification. *IEEE Transactions on Systems, Man, and Cybernetics*, 6(4):269–285.
- Woodcock, C., Strahler, A., and Jupp, D. (1988a). The use of variograms in remote sensing: I. scene models and simulated images. *Remote Sensing of the Environment*, 25:323–348.
- Woodcock, C., Strahler, A., and Jupp, D. (1988b). The use of variograms in remote sensing: II. real digital images. *Remote Sensing of the Environment*, 25:349–379.
- Woodcock, C. E. and Strahler, A. H. (1987). The factor of scale in remote sensing. *Remote Sensing of the Environment*, 21:311–332.
- Woods, J. W. (1972). Two-dimensional discrete Markovian fields. *IEEE Transactions on Information Theory*, 18(2):232–240.
- Wu, S. (1987). Potential application of multipolarization SAR for pine-plantation biomass estimation. *IEEE Transactions on Geoscience and Remote Sensing*, 25(3):403–409.

Appendix A

SAR Geometry and Resolution

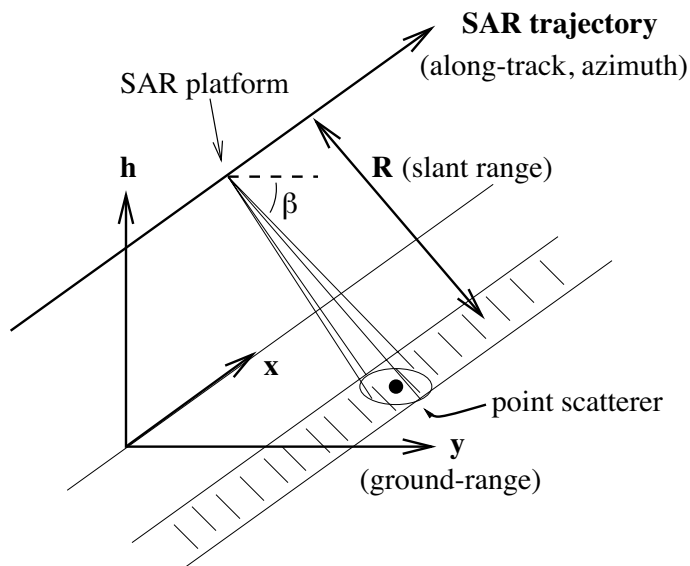


Figure A.1: SAR geometry.

In Figure A.1 the geometry of a SAR system is depicted. The distance from a point on the platform's trajectory to a scatterer (on the ground) is R . The height of the platform is h and y is the horizontal distance from the target to the platform. The axis along the flight path is indicated by x . As the platform moves it emits frequency modulated (FM) signals, called *chirps*, and receives the backscatter or echos (Cenzo, 1981; Fitch, 1988).

SAR is a ranging device. By recording when echos are received, the slant-range of those scatterers can be determined. A signal emitted from the SAR platform would travel a distance of $2R$ in a time of t at a speed of c (speed of light). Therefore

$$R = \frac{ct}{2} \quad (\text{A.1})$$

If two echos return within a very short time frame, say, less than ρ_t , the individual echos can not be resolved because they overlap. If two echos can be resolved in time, they must be separated (in time) by more than ρ_t , the *time resolution*. Therefore, with appropriate time resolution, the ground-range of any echo can be determined and assigned a position on the image by using the slant-range and angle β .

How does the system recognize an echo? The SAR system correlates the echo with a signal which is identical to the original transmitted signal. When the correlation function has a peak, the echo and the signal are very similar and one can be sure that an echo has indeed returned from a strong scatterer (a scatterer that reflects the signal well). The FM signal has a large maximum at zero and rapidly falls as the autocorrelation function moves away from zero. This makes the FM signal ideal for correlating the signal with an echo. If the correlation does not have a large

enough peak, it is deduced that no strong scatterer is present. This, however does not mean that no scatterers were present, it suggests only that no strong scatterers were present.

With the proper time resolution and using correlation, the system is able to record the response and position of all the scatterers along a range-line (the y axis). To form an image, the echos at different x positions along the flight path are collected, and an image can be built up.

Since the platform is moving, with velocity v , the signal reflected by a scatterer will be recorded several times. This happens because the pulse illuminates an elliptical shape on the surface of the earth and the ellipses from different pulses will partially overlap. Therefore, each echo from same scatterer (but different pulses) will experience a Doppler shift. If the scatterer is being approached the frequency shift is positive and if the scatterer is being left the frequency shift is negative. To form an azimuth-line of imagery using the Doppler shifts, the echos from the same scatterer, but illuminated from several different angles, are aligned and the processed into one echo.

A.1 Range Resolution

This paragraph explains how the bandwidth of the chirp is related to the slant-range resolution. First note that the inverse of the time resolution is approximately equal to the bandwidth of the signal, W .

$$\rho_t^{-1} \approx W \quad (\text{A.2})$$

This is necessary to ensure the echos do not overlap. Also the range resolution ρ_r is related to the time resolution by (same relationship in Equation (A.1))

$$\rho_r = \frac{c\rho_t}{2} \quad (\text{A.3})$$

Then combining these two equations, one can see that the range resolution is inversely proportional to the signal bandwidth.

$$\rho_r = \frac{c}{2W} \quad (\text{A.4})$$

A.2 Azimuth Resolution

This section explains why the azimuth resolution is independent of range and wavelength. Consider an equation which relates the azimuth resolution to the Doppler bandwidth and the velocity of the platform.

$$\rho_x = \frac{v}{\Delta f_D} \quad (\text{A.5})$$

The Doppler bandwidth is denoted by Δf_D and azimuth resolution is denoted by ρ_x . Furthermore, the Doppler bandwidth is related to the velocity of the platform, the wavelength of the radiation, λ , and the angle over which the scatterer is illuminated, α , in the following equation.

$$\Delta f_D \approx \frac{2v\alpha}{\lambda} \quad (\text{A.6})$$

The azimuth resolution is independent of range and wavelength because

$$\alpha \approx \frac{\lambda}{D} \quad (\text{A.7})$$

where D is the azimuth dimension of the antenna. Substituting Equations (A.7) and (A.6) into (A.5) yields

$$\rho_x \approx \frac{D}{2} \quad (\text{A.8})$$

which is independent of range or wavelength. This equation implies that the azimuth dimension of the antenna is directly proportional to the azimuth resolution.

Appendix B

GIS Stand Classes

The GIS polygon attribute data was in the form of codes which represented classes of forestry parameters. This appendix outlines the GIS codes and classes that were used in this thesis.

Species Codes and Classes		
1	A	Cottonwood
2	B	Balsam
3	C	Western red cedar
4	Cy	Yellow cedar
6	D	Alder
7	F	Douglas fir
8	H	Hemlock
10	Pl	Lodgepole pine
11	Pw	White pine
12	S	Spruce

Age Codes and Classes	
1	1-20 years
2	21-40 years
3	41-60 years
4	61-80 years
5	81-100 years
6	101-120 years
7	121-140 years
8	141-250 years
9	250+ years

Height Codes and Classes	
1	1-10 m
2	10.1-20 m
3	20.1-30 m
4	30.1-40 m
5	40.1-50 m
6	50.1-60 m
7	60.1-70 m
8	70.1-80 m

Stocking Codes and Classes	
1	dense
2	normal
3	open